Eur. Phys. J. C 53, 429–446 (2008)
DOI 10.1140/epjc/s10052-007-0472-7

THE EUROPEAN PHYSICAL JOURNAL C

Regular Article – Theoretical Physics

Wedgebox analysis of four-lepton events from neutralino pair production at the LHC

G. Bian[1], M. Bisset[1,a], N. Kersting[2], Y. Liu[2], X. Wang[2]

[1] Center for High Energy Physics and Department of Physics, Tsinghua University, 100084 Beijing P.R. China
[2] Physics Department, Sichuan University, 610064 Changdu, P.R. China

Received: 27 March 2007 / Revised version: 26 September 2007 /
Published online: 4 December 2007 –

Abstract. A 'wedgebox' plot is a two-dimensional scatter-plot of two invariant mass quantities. Here $pp \to e^+e^-\mu^+\mu^- + \not{E}$ signature LHC events are analyzed by plotting the di-electron invariant mass versus the di-muon invariant mass. Data sets of such events are obtained across the MSSM input parameter space in realistic event-generator simulations, including cuts designed to remove SM backgrounds. Their study reveals several general features. Firstly, regions in the MSSM input parameter space where a sufficient number of events are expected so as to be able to construct a clear wedgebox plot are delineated. Secondly, the presence of box shapes on a wedgebox plot either indicates the presence of heavy Higgs bosons' decays or restricts the location to a quite small region of low μ and M_2 values, $\lesssim 200$ GeV, a region denoted as the 'lower island'. In this region, wedgebox plots can be quite complicated and change in pattern rather quickly as one moves around in the (μ, M_2) plane. Thirdly, direct neutralino pair production from an intermediate Z^{0*} may only produce a wedge shape since only $\widetilde{\chi}^0_2\widetilde{\chi}^0_3$ decays can contribute significantly. And fourthly, a double-wedge or wedge-protruding-from-a-box pattern on a wedgebox plot, which results from combining a variety of MSSM production processes, yields three distinct observed endpoints, almost always attributable to $\widetilde{\chi}^0_{2,3,4} \to \widetilde{\chi}^0_1\ell^+\ell^-$ decays, which can be utilized to determine a great deal of information about the neutralino and slepton mass spectra and related MSSM input parameters. Wedge and double-wedge patterns are seen in wedgebox plots in another region of higher μ and M_2 values, denoted as the 'upper island'. Here the pattern is simpler and more stable as one moves across the (μ, M_2) input parameter space.

1 Introduction

The large hadron collider (LHC) is scheduled to begin operation next year, at which time the predictions of models of particle physics beyond the standard model (SM), especially supersymmetry (SUSY), will be confronted with challenging experimental constraints. SUSY predicts heavy scalar counterparts, or superpartners, to the SM fermions, as well as fermionic superpartners to the SM bosons – both the spin-1 gauge bosons and the spin-0 Higgs bosons (SUSY requires more than one Higgs boson). These new states are known collectively as sparticles. Colorless sparticles, including the neutralinos ($\widetilde{\chi}^0_i$) and charginos ($\widetilde{\chi}^\pm_j$) – the neutral and charged, respectively, superpartners of admixtures of the gauge and Higgs bosons – are generally expected to be somewhat lighter than their colored brethren, the gluinos ($\tilde{g}$) and squarks ($\tilde{q}$). Nonetheless the colored sparticles are expected to have the larger production cross-sections, unless they are much (an order of magnitude or so) more massive. Yet this is precisely what occurs in some hypothesized SUSY-breaking scenarios: the squarks and gluinos have masses on the scale of several TeV, while neutralinos and charginos have masses on the scale of several hundred GeV (or less). Therefore a study of these sparticles' direct production modes is warranted. Moreover, aside from their direct production modes, colorless sparticles inevitably appear *indirectly* in any colored sparticle production process through the sometimes complicated decay chains of the gluinos and squarks. Thus, determining the masses and couplings of the neutralinos and charginos is crucial to understanding almost any SUSY events that may emerge at the LHC.

In the R-parity-conserving minimal supersymmetric standard model (MSSM), sparticles must be pair-produced, and the lightest sparticle (the LSP), for which the preferred candidate is generally the lightest neutralino ($\widetilde{\chi}^0_1$), is stable. The focus of this study is the neutralinos, of which there are four in the MSSM, and in particular the heavier three ($\widetilde{\chi}^0_i$, $i = 2, 3, 4$ in order of increasing mass) – which are expected to decay, either directly or indirectly, into the LSP. MSSM neutralino pair production at the LHC can in general occur via three avenues herein known as direct, Higgs-mediated, and colored sparticle cascade decays, as shown in Fig. 1. Cascade decays were studied in [1], while [2, 3] focused on Higgs-mediated decays. The present study enlarges the focus of [2, 3] to also encompass

[a] e-mail: bisset@mail.tsinghua.edu.cn

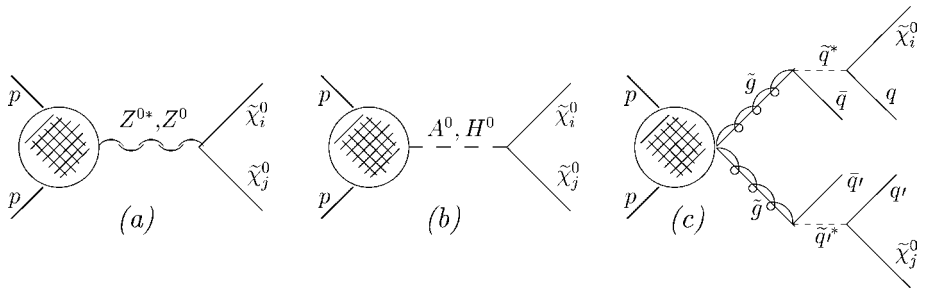

Fig. 1. Feynman diagrams for heavy ($i, j = 2, 3, 4$) neutralino pair production mechanisms: **a** 'direct' production via an EW gauge boson; **b** Higgs-mediated production; and **c** production via cascade decays of gluinos (shown here) or squarks (make squarks in diagram on-mass shell and remove the gluinos and the connected quarks)

the direct production channel via the electroweak (EW) Z^0 gauge boson, which formed an unavoidable and often significant background in the study of [2, 3]. This direct avenue is most dominant when the colored sparticles and the extra Higgs bosons of the MSSM are quite massive (such as if squark, gluino, and pseudoscalar Higgs MSSM input masses are set around the TeV scale).

In an LHC detector, each short-lived heavier neutralino produced must decay into SM particles plus an LSP. Invisible LSPs (along with any SM neutrinos that may be present) generate the tell-tale SUSY missing energy signature. Rates for the observed final state SM particles and the distributions of their energies and momenta will depend on MSSM (especially neutralino) masses and couplings. It would be simplest to examine final states that are produced by only one unique pair of neutralinos, and, on top of this, via only one of the aforementioned neutralino pair production avenues, though clearly nature is neither obliged nor expected to make LHC analyses so straightforward.

In the present study, as well as in [1], the signature examined is neutralino pair decays into an electron–positron pair, a muon–antimuon pair, and missing energy (and possibly jets): $pp \to \widetilde{\chi}_i^0 \widetilde{\chi}_j^0 \to e^+e^-\mu^+\mu^- + \not{E}(+n\,\text{jet})$, where all leptons are hard and isolated (exact conditions for these requirements will be given later). The rationales for choosing this particular final state are two-fold: first, in the hadronically noisy environment of the LHC, multi-lepton signals have minimal SM backgrounds and thus tend to be easier to identify. Second, assuming the neutralinos to proceed to this final state via one of the following decay chains:

$$\widetilde{\chi}_i^0 \to \{Z^0, Z^{0*}\} + \widetilde{\chi}_1^0 \to \ell^+\ell^- + \widetilde{\chi}_1^0\,, \tag{1}$$

$$\widetilde{\chi}_i^0 \to \ell^\mp + \{\tilde{\ell}^\pm, \tilde{\ell}^{\pm *}\} \to \ell^+\ell^- + \widetilde{\chi}_1^0\,, \tag{2}$$

where $\ell = e$ or μ, the dilepton invariant masses are cleanly bounded by

$$0 < M_{i1}(\ell^+\ell^-) < m_{\widetilde{\chi}_i^0} - m_{\widetilde{\chi}_1^0}\,, \tag{3}$$

$$0 < M_{i1}(\ell^+\ell^-) < m_{\widetilde{\chi}_i^0} \sqrt{1 - \left(\frac{m_{\tilde{\ell}}}{m_{\widetilde{\chi}_i^0}}\right)^2} \sqrt{1 - \left(\frac{m_{\widetilde{\chi}_1^0}}{m_{\tilde{\ell}}}\right)^2}\,, \tag{4}$$

depending on whether the decays are 3-body (via Z^{0*} or $\tilde{\ell}^{\pm *}$) or 2-body via an on-mass-shell charged slepton, respectively. A 2-body decay via an on-mass-shell Z^0 leads to $M_{i1}(\ell^+\ell^-) = M_Z$, which is non-trivial to extract from SM backgrounds. The fact that the dilepton invariant mass spectrum basically increases as one runs up in mass to the upper kinematical edge [4] greatly facilitates a precise determination of this bound. Then, if the electron and muon pairs always come from one particular ij-combination of neutralinos, plotting their dilepton invariant masses against each other in a two-dimensional $M(e^+e^-)$ versus $M(\mu^+\mu^-)$ Dalitz-like plot [1] will yield either a box (for $i = j$) or wedge shape (for $i \neq j$) with hard kinematical edges at (3) or (4). Note that here the lepton pairs are required to be of different flavors to facilitate proper pairings.

However, the situation is complicated at the LHC (where the partonic center-of-mass is not fixed) by the fact that several different ij-combinations may be produced – each at a different rate. Thus the plot will in general consist of a superposition of various boxes and wedges, hereafter designated as a 'wedgebox' plot. The power of the wedgebox plot technique manifests itself in precisely such a situation, since, given a sufficient number of events, the endpoints of (3) and (4) may each be cleanly identified, and, from the relative densities of easily-defined sectors [1] of the wedgebox plot, production ratios such as $\sigma(pp \to \widetilde{\chi}_i^0 \widetilde{\chi}_j^0)/\sigma(pp \to \widetilde{\chi}_k^0 \widetilde{\chi}_l^0)$, may be inferred (since the expected distribution of individual event points within a wedge or box from a particular ij-combination is fairly simple to model mathematically [4]). This information may then be used to constrain the neutralino masses and couplings and hence the fundamental MSSM input parameters (MSSM IPs) of the neutralino mass matrix. Wedgebox plots are hence superior to more traditional one-dimensional invariant mass histograms for this four-lepton signature.

Neutralino decay modes other than those included in (1) and (2) are possible. Firstly, a neutralino may choose to not decay to the $\widetilde{\chi}_1^0$ LSP as shown in these reactions, but rather to an intermediate mass neutralino, as in $\widetilde{\chi}_4^0 \to \widetilde{\chi}_3^0 + \ell^+\ell^-$, $\widetilde{\chi}_4^0 \to \widetilde{\chi}_2^0 + \ell^+\ell^-$, or $\widetilde{\chi}_3^0 \to \widetilde{\chi}_2^0 + \ell^+\ell^-$. This additional daughter neutralino (or neutralinos) would subsequently decay to the $\widetilde{\chi}_1^0$ without producing any more leptons. The significant presence of such decay chains would introduce 'stripes' in the wedgebox plot, further enriching its structure: including the possibility of these stripes leads to 178

distinct[1] wedgebox plots within the MSSM framework. Typically though, such extended decay chains are unimportant, or at least sub-dominant. Four-lepton decays from a single neutralino $\widetilde{\chi}_i^0 \to \ell^+\ell^-\widetilde{\chi}_k^0 \to \ell^+\ell^-\widetilde{\chi}_1^0\ell'^+\ell'^-$ (here the aforementioned daughter neutralino does yield a lepton pair from its decay while the other production neutralino yields no leptons) are also possible, but their rates of occurrence are smaller yet. With inclusion of these stripes, and in the limit of infinite luminosity, a wedgebox plot from the LHC would consist of a 6×6 checkerboard in the $M(e^+e^-), M(\mu^+\mu^-)$ plane (where the location of the lines are related to the six possible mass differences between the four MSSM neutralinos). However the actual integrated luminosity of the LHC is limited, by a conservative estimate, to roughly $300\,\mathrm{fb}^{-1}$ over its lifetime, and generally this will not be enough to resolve the full checkerboard. Instead a specific combination of boxes and wedges will be observed in the wedgebox plot based on the dominant production modes for neutralino pairs and the dominant neutralino decay modes. Identifying these dominant modes will strongly constrain the MSSM IPs.

Secondly, and more worrisome from the point of view of the present analysis, are processes involving charginos. A neutralino may decay to the LSP via an intermediate chargino: $\widetilde{\chi}_i^0 \to \ell^+\nu + \widetilde{\chi}_1^- \to \ell^+\nu\ell'^-\bar{\nu}' + \widetilde{\chi}_1^0$. In such decays, hereafter designated as 'mavericks', the dilepton invariant masses are not simply bounded as in (3) and (4). Fortunately, such mavericks generally constitute a small minority of the events (especially for choices of the MSSM IPs which will be found to be of particular interest) leading to a diffuse 'halo' on a wedgebox plot, which is superimposed on the desired sharp box and wedge structure. Also, the $e^+e^-\mu^+\mu^- + \not{E}$ final state may result from $\widetilde{\chi}_i^\pm\widetilde{\chi}_j^\mp$ chargino pair production, with $\widetilde{\chi}_i^\pm \to \ell\ell\ell' X + \widetilde{\chi}_1^0$ and $\widetilde{\chi}_j^\mp \to \ell' Y + \widetilde{\chi}_1^0$ (where X and Y are SM final state particles other than ℓs, typically including neutrinos, and intermediate states may involve charged sleptons or sneutrinos). Such '$3+1$' events are also lumped into the maverick category. Thus a maverick event is any $e^+e^-\mu^+\mu^-$ event where members of a same-flavor lepton pair arise disjointly rather than as in[2] (1) or (2). Chargino–neutralino production may yield final states with five charged leptons or four charged leptons and a charged quark pair (typically leading to jets) to balance charge. For the former, if the extra lepton is too soft or not isolated or lost down the beam pipe, or, for the latter, if a jet cut fails to exclude the event, then chargino–neutralino production may also yield $e^+e^-\mu^+\mu^- + \not{E}$ events. Charginos, especially $\widetilde{\chi}_2^\pm$, may also decay into unstable neutralinos (rather than the other way around as above): $\widetilde{\chi}_i^+ \to \widetilde{\chi}_j^0 + W^+ \to \ell^+\ell^-\widetilde{\chi}_1^0 + q\bar{q}'$. Here this dilepton invariant mass would fit into the expected framework, so as not to interfere with endpoint studies (though presence of such a process would skew attempts to discern neutralino pair production rates from event population studies; note also the presence of quarks that may yield unacceptable jet activity, or, if the W^+ decays leptonically, an extra lepton would need to be lost as above). Another possibility is $\widetilde{\chi}_2^\pm \to \widetilde{\nu}\ell^\pm \to \widetilde{\chi}_1^\pm\ell^\mp\ell^\pm \to \widetilde{\chi}_1^0\ell^\mp\ell^\pm W^\pm$ which would give kinematic edges similar to (3) or (4) (replacing $m_{\widetilde{\chi}_{1,i}^0}$ with $m_{\widetilde{\chi}_{1,2}^\pm}$ and $m_{\widetilde{\ell}}$ with $m_{\widetilde{\nu}}$). The presence of the above decay chains in an event would not invoke the maverick designation. Again, though, such processes are expected to have only modest rates in regions of phenomenological interest.

As noted above, colored sparticle masses may be pushed up above or around the TeV scale to prevent production rates from the cascade channel (see Fig. 1c) from swamping the other production modes. In [1] it was shown in full event-generator level simulations that $\sim 500\,\mathrm{GeV}$ squarks and gluinos led to the overwhelming domination of the cascade channel for the $e^+e^-\mu^+\mu^- + \not{E}$ + jets signature. Backgrounds were found to be nominal and signal rates high enough to produce crisp wedgebox plots over a large range of the MSSM IPs associated with neutralino characteristics. This study also showed that, as expected, cascade events virtually always have associated jet activity. Thus a limit on the maximum number of jets or on the maximum allowable jet energy in an event can remove most of the cascade events while leaving many of the direct and Higgs-mediated events (one may speak of demanding that the events be 'hadronically quiet'). As seen above, such a cut may also reduce the effects from maverick events. Subsequent detailed simulation studies explicitly demonstrate that a cut on jet energy can eliminate the cascade channel over the entire phenomenologically-interesting range of colored sparticles' masses.

This would leave the direct and Higgs-mediated avenues to disentangle. Note that for both these avenues the two neutralinos arise from the decay of a single fundamental particle, whereas in the cascade avenue the neutralinos are produced independently (and possibly from decays of different colored sparticles – e.g., one neutralino from a gluino and the other from a particular species of squark). Thus couplings of the EW sector of the MSSM (excluding those associated with sleptons for the moment), which are presumably determinable solely from the EW MSSM inputs to the neutralino mixing matrix, are better scrutinized via a sample of events from the direct and Higgs-mediated avenues with the cascade avenue events filtered out. Study [2, 3] focused on the Higgs-mediated avenue and found that direct avenue production formed a background to the sought-for heavy Higgs boson signals that was difficult if not impossible to remove by any set of kinematical cuts. To focus instead on the direct channel, one could by hand simply choose the Higgs input parameter (generally chosen as the pseudoscalar Higgs mass, m_A) large enough (in the vicinity of a TeV) to shut down the Higgs-mediated avenue. Nature may not respect this choice though. The present study avoids these dilemmas by simply not attempting to cut away either avenue: the wedgebox plot consists of a superposition of shapes from each of the two different avenues. Each avenue may contribute different shapes, if so signaling their respective presences,

[1] For example, $\widetilde{\chi}_2^0\widetilde{\chi}_2^0$, $\widetilde{\chi}_3^0\widetilde{\chi}_3^0$ and $\widetilde{\chi}_4^0\widetilde{\chi}_4^0$ processes each separately give a box, so a wedgebox plot containing only $\widetilde{\chi}_2^0\widetilde{\chi}_2^0$ is not 'distinct' from a wedgebox plot containing only one of the other two processes.

[2] For 'stripe' events, which are not mavericks, $\widetilde{\chi}_1^0$ would be replaced by $\widetilde{\chi}_j^0$, $j \neq 1$ in (1) or (2).

and, for favorable choices of MSSM IPs (as will be delineated herein), three kinematic edges – as per (3) or (4) – may be seen, strongly constraining the neutralino masses and IPs.

The remainder of the paper has the following organization: in Sect. 2 the MSSM IP space is scanned for the inclusive rate, that is, the rate before the imposition of any kinematical cuts, of the neutralino pair-produced $e^+e^-\mu^+\mu^-\not\!\!E$ signature via the direct and Higgs-mediated avenues to identify regions of the space where the signature is potentially observable. Guided by these estimates, Sect. 3 then follows with more detailed full event-generator Monte Carlo (MC) simulations to carefully analyze the salient regions of the MSSM IP space. Results from the parameter space scans and the MC simulations are further expounded upon in Sect. 4, and finally Sect. 5 gives conclusions to be drawn from this work.

2 Parameter space scans

Before running a full event-generator MC simulation of neutralino pair production at selected points in the MSSM IP space, it is efficient to first obtain some estimates of the typical signal and background rates. Here signal refers to direct production or Higgs-mediated avenues of neutralino pair production, $pp \to Z^* \to \widetilde{\chi}_i^0\widetilde{\chi}_j^0$ or $pp \to H^0, A^0 \to \widetilde{\chi}_i^0\widetilde{\chi}_j^0$. The intermediate Higgs boson is assumed to be on-mass-shell. This is consistent with what is done in current MC programs to be used later. A similar study of Higgs boson decays into sleptons at the LHC found effects from also allowing the Higgs boson to be off-mass-shell to be quite modest [5]. If the cascade avenue is shut down either by making the colored sparticles very massive or by an appropriate jet cut, then the main MSSM backgrounds are from chargino and slepton production. Processes not studied in this initial analysis therefore include minor players such as $t\bar{t}h$, $tH^\pm$, $tbH^\pm$, etc., and all SM backgrounds. Though these all may yield $e^+e^-\mu^+\mu^- + \not\!\!E$ events, their contributions may be rendered negligible by a suitable set of cuts, as shown in [2, 3] and in the MC studies to follow. In particular, SM processes may be virtually eliminated by demanding a sufficient amount of missing energy, hard leptons that are isolated, and limits on jet activity – save for Z^0Z^{0*}-induced events, which lead (after cuts and for 300 fb^{-1} integrated luminosity) to a few dozen events along the 'Z-lines' on a wedgebox plot.

The MSSM IPs that factor directly in the neutralino and chargino mixing matrices are $\tan\beta$, the ratio of the Higgs boson vacuum expectation values, μ, the SUSY higgsino mass parameter, and M_2, the soft SUSY-breaking $\mathrm{SU(2)_L}$ gaugino mass (in what follows, M_1, the soft SUSY-breaking $\mathrm{U(1)}_Y$ gaugino mass, is assumed to be fixed by M_2 and the gauge unification constraint $M_1 = 5/3\tan^2\theta_\mathrm{W} M_2$). These MSSM IPs are allowed to take values in the ranges: $2 < \tan\beta < 50$ (upper limit guided by perturbativity), and 100 GeV $< \mu, M_2 <$ 500 GeV – here the lower bound is set to avoid LEP-excluded light colorless sparticles and the upper bound to avoid heavier neutralinos ($\widetilde{\chi}_3^0$ and $\widetilde{\chi}_4^0$) too massive to generate significant production rates.

Higgs-mediated events are sensitive to the pseudoscalar Higgs mass m_A: as m_A increases, phase space opens up for more $\widetilde{\chi}_i^0\widetilde{\chi}_j^0$ decay channels; however, the cross section for $pp \to H^0, A^0$ drops precipitously. Thus the preferred range for a potentially meaningful contribution from the Higgs-mediated avenue is 300 GeV $\lesssim m_A \lesssim$ 700 GeV.

Also of crucial importance to the neutralino decays into charged leptons are the slepton sector MSSM IPs. Each flavor generation has two soft slepton mass inputs $m_{\widetilde{\ell}_{\mathrm{L,R}\,i}}$ $(i = e, \mu, \tau)$[3] Most models of SUSY-breaking generate little splitting between the inputs of the first two generations, and thus, for simplicity, these inputs are set degenerate. This assumption makes the wedgebox plots virtually symmetric under the interchange of the axes, while relaxing this assumption may make the wedgebox plot asymmetric (for instance, the 'boxes' could become 'rectangles'). The third generation stau inputs are however distinctive in many SUSY-breaking scenarios, and herein these inputs are elevated (by hand) by 100 GeV over the degenerate selectron and smuon mass inputs. The lighter selectrons and smuons then favor, via reaction (2), events of the signature type over those containing tau leptons. This enhances the signal rates, while at the same time reducing one additional source of maverick events (stemming from events with leptonic tau decays). Conversely, measuring the asymmetry and maverick halo density of the observed wedgebox plot would provide information about the slepton sector mass inputs. This leaves two parameters from the slepton sector to vary: the degenerate soft SUSY-breaking mass input for the right sleptons of the first two generations (the superpartners of the right-handed electron and muon), $m_{\widetilde{\ell}_\mathrm{R}}$, and the corresponding mass input for the left sleptons, $m_{\widetilde{\ell}_\mathrm{L}}$. If both these slepton masses are set very high, then neutralino decays via gauge bosons as in reactions (1) totally dominate and the leptonic branching ratios (BRs) of the neutralinos are simply those of the SM gauge bosons. This is insufficient for generating enough events for detection of the signature. Thus positive results in this work depend on sleptons being reasonably light ($\lesssim$ 350 GeV) – a condition that fits comfortably with the neutralino MSSM IPs under consideration. These light sleptons will then enhance the leptonic BRs of the neutralinos [6]. In addition to generating reactions like (2), light slepton mass inputs can also generate

$$\widetilde{\chi}_i^0 \to \bar{\nu} + \tilde{\nu} \to \bar{\nu}\nu + \widetilde{\chi}_1^0 \tag{5}$$

decay chains which (hereafter designated as 'spoiler modes') act to diminish BRs of modes yielding the 4ℓ signal.[4] Of particular importance to the present study is

[3] There are also trilinear soft inputs $A_{\ell i}$, but these always come attached to a Yukawa coupling and thus are irrelevant for the first two generations.

[4] Another potential decay mode is $\widetilde{\chi}_i^0 \to \widetilde{\chi}_1^0 h^0$, with $h^0 \to b\bar{b}$. Here leptonic decays are absent; however, b-tagging may allow for the reconstruction of $M(b\bar{b})$. This decay mode is prominent in several studies at selected mSUGRA points [7–10].

the situation where $m_{\tilde{\nu}} < m_{\widetilde{\chi}_2^0} < m_{\tilde{\ell}^\pm}$; here $\widetilde{\chi}_2^0$ will mainly decay via an on-shell sneutrino and its BR into a pair of charged leptons is highly suppressed, killing the 4ℓ signal. If SUSY-breaking processes respect $SU(2)_{\rm L}$ symmetry, then the sneutrino and left charged slepton of a given flavor have the same soft input mass parameter (their masses are split by small D-term contributions). Since the sneutrino mass is thus tied to $m_{\tilde{\ell}_{\rm L}}$, lowering $m_{\tilde{\ell}_{\rm R}}$ relative to $m_{\tilde{\ell}_{\rm L}}$ tends to suppress spoiler modes and improve the signal rate.

A private code was used normalized by cross-sections input from the event generator ISAJET [11, 12] to perform a scan over the μ and M_2 neutralino IPs for the signature $\sigma(pp \to X) \times {\rm BR}(X \to e^+e^-\mu^+\mu^-)$ where X represents the intermediate states (as in Fig. 1a or b in the case of the signal). Other MSSM IPs were fixed as follows: $\tan\beta = 10$, $m_A = 600\,{\rm GeV}$, $m_{\tilde{g},\tilde{q}} = 1000\,{\rm GeV}$, $m_{\tilde{e},\tilde{\mu}} = 150\,{\rm GeV}$, $m_{\tilde{\tau}} = 250\,{\rm GeV}$, and vanishing soft A-terms. In this initial parton-level analysis, the mere presence of exactly the four leptons in the signature is all that is required with no demands whatsoever made upon their kinematical properties (e.g., transverse momenta or pseudorapidity). Any effects from the underlying spectator event are neglected. By contrast, in the full event-generator MC analysis to follow, appropriate cuts on the leptons' kinematical properties will be applied, meaning that the numerical results of the initial analysis are overestimates. The initial analysis also demands no quarks in the final state, where only particles resulting from the primary parton-level interaction are taken into account. On the other hand, in the full event-generator MC analysis quark remnants from the colliding protons must at the very least yield quarks in the final state (though these typically lie close to the beam axis). Thus at best a lower bound can be set upon hadronic or jet activity in the final state, which would tend to make the results of the initial analysis underestimates of the event generator MC results. Of these two differences between the two analyses, the former effect is expected to be more significant. Thus the results from the initial analysis may be treated as upper bounds of what may be expected from the subsequent more realistic (and also far more computing time-intensive) event-generator MC studies.

Figure 2 shows the results[5], assuming an integrated luminosity of $300\,{\rm fb}^{-1}$. The lower and upper shaded areas are excluded by LEP searches (restricting[6] $m_{\widetilde{\chi}_1^\pm}$) and cosmological/dark matter considerations (i.e., require $\widetilde{\chi}_1^0$ to be the LSP), respectively. Figure 2a shows what may be expected from the direct channel. Of the six possible $\widetilde{\chi}_i^0\widetilde{\chi}_j^0$ pairs ($i, j = 2, 3, 4$), only the $\widetilde{\chi}_2^0\widetilde{\chi}_3^0$-combination leads to a significant number of events (set as 100 events). Phase space suppression renders the $\widetilde{\chi}_i^0\widetilde{\chi}_4^0$ channels negligible. The rate for $\widetilde{\chi}_2^0\widetilde{\chi}_2^0$ is suppressed since, in the pertinent region of the (μ, M_2) parameter space, the $\widetilde{\chi}_2^0$ has approximately equal higgsino components and the $Z\widetilde{\chi}_2^0\widetilde{\chi}_2^0$ coupling[7] vanishes due to the cancellation between the contributions from these two higgsino components. An analogous suppression occurs with the $\widetilde{\chi}_3^0\widetilde{\chi}_3^0$ mode, along with substantial phase space suppression. Note that there are too few events at either high M_2 and/or high μ to meet the significance criterion due to the small size of $\sigma(pp \to \widetilde{\chi}_2^0\widetilde{\chi}_3^0)$. In the remaining portion of the (μ, M_2) MSSM IP plane dominant sneutrino spoiler modes confound $\widetilde{\chi}_2^0 \to \ell^+\ell^-\widetilde{\chi}_1^0$ decays in a more or less hyperbolic strip of low signal event rates passing through $(\mu, M_2) = (200\,{\rm GeV}, 200\,{\rm GeV})$, leaving two signal event rate peaks at $(\mu, M_2) \simeq (200\,{\rm GeV}, 300\,{\rm GeV})$ and $(150\,{\rm GeV}, 175\,{\rm GeV})$.[8]

Figure 2b gives the results for the Higgs-mediated channels. Rates everywhere exceed those of the direct $\widetilde{\chi}_2^0\widetilde{\chi}_3^0$ production mode since the mechanism suppressing $\widetilde{\chi}_2^0\widetilde{\chi}_2^0$ in the direct channel does not apply to the Higgs' couplings. However the optimal point in the plane is in roughly the same location, around $(\mu, M_2) \simeq (200\,{\rm GeV}, 275\,{\rm GeV})$, largely due to the aforementioned sneutrino spoiler mechanism turning on as one moves off this peak. These features directly follow from the choices made for m_A and $\tan\beta$ (600 GeV and 10, respectively). As found in [2, 3], Higgs decays to $\widetilde{\chi}_2^0\widetilde{\chi}_2^0$ tend to dominate for larger values of μ. This means that Higgs-mediated processes can lead to a box, whereas the direct avenue is expected to produce a wedge. On the other hand, [2, 3] also found that decays including the heavier neutralinos $\widetilde{\chi}_3^0$ and $\widetilde{\chi}_4^0$ may be very significant or even dominate for smaller values of μ (assuming m_A is sufficiently large). Thus more complicated wedgebox plots may be expected from Higgs-mediated processes at lower values of μ (and higher values of m_A).

The most significant SUSY backgrounds involve charginos. Figures 2c and d display expected 5- and 4-lepton event rates from $pp \to \widetilde{\chi}_i^0\widetilde{\chi}_j^\pm$ and $pp \to \widetilde{\chi}_i^\pm\widetilde{\chi}_j^\mp$, respectively. Here the $\widetilde{\chi}_i^0\widetilde{\chi}_j^\pm$ pair is required to produce five leptons, and then one lepton would have to be 'lost'. Losing the extra lepton is *not* taken into account in the rates shown in c, and thus the background rate due to this process

[5] Note that in this plot, as well as in other ones to follow, $\mu > 0$ is chosen. While analogous plots for $\mu < 0$ are not quite symmetric to the $\mu > 0$ plots shown here, substantive differences are few with the same features appearing at slightly shifted values of $|\mu|$.

[6] For physical sneutrino masses below 200 GeV, destructive interference from a t-channel sneutrino exchange diagram with the normal s-channel diagram for e^+e^--collider chargino pair production lowers the bound given by LEP experimental groups [13] from $m_{\widetilde{\chi}_1^\pm} > 103\,{\rm GeV}$ (singly hatched bound on plots) to $m_{\widetilde{\chi}_1^\pm} > 85\,{\rm GeV}$ (doubly hatched bound on plots). A true experimentalist's bound for the MSSM IP sets considered herein would thus be expected to lie somewhere within the singly hatched zone.

[7] In the notation of [14], this term is $\langle Z|\widetilde{\chi}_i^0\widetilde{\chi}_j^0\rangle = (g/2\cos\theta) \times {\rm Re}(N_{i3}N_{j3}^* - N_{i4}N_{j4}^*)$. The crucial minus sign in this equation arises from the different hypercharges of the two MSSM Higgs doublets. If $i = j$, this leads to a strong tendency for the two terms to cancel each other. However, for $i = 2$ and $j = 3$, as in direct $\widetilde{\chi}_2^0\widetilde{\chi}_3^0$ production, the signs of either N_{23} and N_{33} *or* N_{24} and N_{34} – *but not both* – are opposite over much of the interesting region of the MSSM IP space, and enhancement rather than cancellation ensues.

[8] Though not very discernible on the plots, there is also a very narrow bridge of high rates centered on $(\mu, M_2) \simeq (155\,{\rm GeV}, 245\,{\rm GeV})$. This is where the sneutrino coupling to $\widetilde{\chi}_2^0$ dies, turning off the most important spoiler mode.

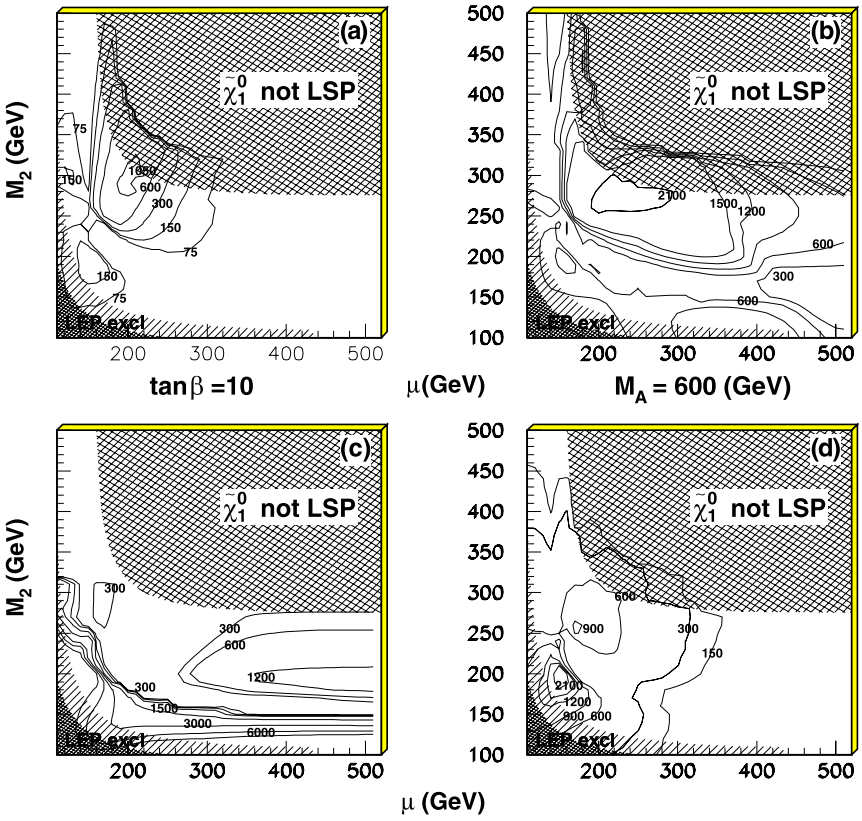

Fig. 2. Number of $e^+e^-\mu^+\mu^-$ events (inclusive rates with no cuts) expected per $300\,\mathrm{fb}^{-1}$ of integrated luminosity from **a** $pp \to \widetilde{\chi}_2^0\widetilde{\chi}_3^0$; **b** $pp \to H^0/A^0$; **c** $pp \to \widetilde{\chi}_i^0\widetilde{\chi}_j^\pm$ and **d** $pp \to \widetilde{\chi}_i^\pm\widetilde{\chi}_j^\mp$. Other MSSM inputs are fixed as $\tan\beta = 10$, $m_A = 600\,\mathrm{GeV}$, $m_{\tilde{e},\tilde{\mu}} = 150\,\mathrm{GeV}$ and $m_{\tilde{\tau}} = 250\,\mathrm{GeV}$. The uncertainty shown in the extent of the LEP excluded region stems from the presence of a relatively light sneutrino (as discussed in a footnote)

is certainly overestimated by this plot. Nonetheless, the plot clearly shows that the largest rates from $\widetilde{\chi}_i^0\widetilde{\chi}_j^\pm$ should come at low values of M_2 (with some preference also for higher values of μ). This is not a region where the direct and Higgs-mediated neutralino pair production processes are expected to yield enough events to sufficiently populate a wedgebox plot. Thus at worst $\widetilde{\chi}_i^0\widetilde{\chi}_j^\pm$ processes would contribute a small minority of the events in a neutralino pair-induced wedgebox plot. As seen from Fig. 2d, chargino pair production is expected to generate a fair number of four-lepton events (typically mavericks), which might act to cloud the neutralino-based features of the wedgebox plot. Light charginos are generally expected to have larger cross-sections at the LHC than neutralinos. Fortunately, $\widetilde{\chi}_1^+\widetilde{\chi}_1^-$-production can almost never generate the four-lepton final state. Requiring processes involving the heavier chargino pushes the location for optimal rates from chargino pair production to quite low values of M_2 and μ. This is mostly non-overlapping with the preferred IP space region for neutralino pair-production processes; however, a secondary maximum in the chargino pair rates is seen at $(\mu, M_2) \simeq (200\,\mathrm{GeV}, 250\,\mathrm{GeV})$, and this is in the region where a neutralino pair-induced wedgebox plot would be viable. One possible method for alleviating this problem (not implemented in this work) would be to examine $\ell^+\ell^-\ell^+\ell'^-$ events (since with $\widetilde{\chi}_i^+\widetilde{\chi}_j^-$ one chargino is expected to produce three leptons, while the other chargino produces only one, while with $\widetilde{\chi}_i^0\widetilde{\chi}_j^0$ each neutralino should, with rare exceptions, produce a pair of same-flavor leptons), which should have rates equivalent to $\ell^+\ell^-\ell^+\ell^-$, as the basis for a chargino pair event subtraction scheme [15].

Finally, slepton production also comprises a potentially large background. In [2,3], four-lepton signature events from slepton pair production were found to be even harder to cut away from the desired Higgs-mediated signal than events from direct avenue neutralino pair production, though in that case only enough Higgs-mediated signal events were sought to claim a signal of ~ 20 events after all cuts. In this work, on the other hand, hundreds of events are needed. We discuss this issue at more length in the following section, where it is found that sleptons contribute significantly only at very low values of μ or M_2; i.e., in regions where signal rates are small. However, sleptons are always of paramount importance as intermediates in the decays of the neutralinos to the desired charged leptons.

3 Monte Carlo event-generator analysis

The HERWIG 6.5 [16,17] MC package (which obtains its MSSM input information from ISASUSY [11,12] through the ISAWIG [20] and HDECAY [21] interfaces) is employed to generate realistic LHC events. The CTEQ 6M [18,19] set of parton distribution functions is used with top and bottom quark masses set to $m_t = 175\,\mathrm{GeV}$ and $m_b = 4.25\,\mathrm{GeV}$, respectively. This is coupled with private programs (checked against results in the literature) simulating a typical LHC detector environment. Assuming an integrated luminosity of $300\,\mathrm{fb}^{-1}$, roughly equivalent to several years' high luminosity data from the LHC, the appropriate numbers of events (normalization was accord-

Table 1. Expected number of events at $(\mu, M_2) = (150\,\text{GeV}, 160\,\text{GeV})$ and $(\mu, M_2) = (190\,\text{GeV}, 280\,\text{GeV})$ after successive cuts (for $100\,\text{fb}^{-1}$). The $\widetilde{\chi}\widetilde{\chi}$ entry includes both neutralinos and charginos; at $(190, 280)$ it is in fact overwhelmingly the former, whereas at $(150, 160)$ it is the latter. 'Common bkgs.' do not vary with location in the MSSM IP space; these are essentially the SM backgrounds. Note: the HERWIG [16, 17] event generator was used here

	Process	4ℓ events	$E_{\text{jet}} \leq 50\,\text{GeV}$	$E_{\text{T}}^{\text{miss}}$	$e^+e^-\mu^+\mu^-$
	$Z^{0(*)}Z^{0(*)}$	1645	1416	84	27
	$Z^0 + \text{jet}$	0	0	0	0
Common	$t\bar{t}$	0	0	0	0
bkgs.	$t\bar{t}Z^{0(*)}$	47	7	6	2
	WW	0	0	0	0
	$t\bar{t}h^0$	4	1	1	0
	$\tilde{g}, \tilde{q}$	608	0	0	0
	$\tilde{\ell}$,$\widetilde{\nu}$	647	423	353	125
$(150, 160)$	$\bar{t}H^+$, tH^-	45	9	6	2
	$A^0 + H^0$	$199 + 177$	$114 + 112$	$100 + 96$	$30 + 29$
	$\widetilde{\chi}\widetilde{\chi}$	1932	1215	1040	258
	$\tilde{g}, \tilde{q}$	2298	1	0	0
	$\tilde{\ell}, \widetilde{\nu}$	83	39	35	5
$(190, 280)$	$\bar{t}H^+$, tH^-	198	38	29	9
	$A^0 + H^0$	$574 + 468$	$392 + 322$	$334 + 270$	$135 + 95$
	$\widetilde{\chi}\widetilde{\chi}$	1106	650	527	196

ing to HERWIG-delivered cross-sections) for signal and background processes were generated at an array of points spanning the (μ, M_2) plane.

Signature $e^+e^-\mu^+\mu^-$ events are selected according to the following criteria: the event must have exactly four hard ($p_{\text{T}}^{\ell} > 10, 8\,\text{GeV}$ for $e^{\pm}, \mu^{\pm}$, respectively; $|\eta^{\ell}| < 2.4$), isolated (no tracks of other charged particles in a $r = 0.3$ radians cone around the lepton, and less than 3 GeV of energy deposited into the electromagnetic calorimeter for $0.05\,\text{radians} < r < 0.3\,\text{radians}$ around the lepton) leptons, consisting of exactly one e^+e^- pair and one $\mu^+\mu^-$ pair.

After identifying signature events, the following cuts are then applied:

- substantial missing transverse energy must be present, with $20\,\text{GeV} < \not{E}_{\text{T}} < 130\,\text{GeV}$, and
- no jet reconstructed with an energy E_{jet} greater than 50 GeV.

Jets are defined by a cone algorithm with $r = 0.4$ and must have $|\eta^{\text{j}}| < 2.4$. These cuts are sufficient to eliminate all of the SM backgrounds except that from $Z^{0(*)}Z^{0(*)}$ (and to a much lesser extent, $t\bar{t}Z^{0(*)}$) production.[9] The jet cut efficiently removes events from gluino and squark production. What remains are residual SUSY backgrounds from processes involving charginos ($pp \to \widetilde{\chi}_i^{\pm}\widetilde{\chi}_j^{\pm}$ or $\widetilde{\chi}_i^0\widetilde{\chi}_j^{\pm}$ via SM gauge bosons or Higgs bosons), from charged slepton pair production ($pp \to \widetilde{\ell}^{\pm}\widetilde{\ell}^{\mp}$), and (making a minor contribution) from $pp \to tH^-, \bar{t}H^+$. Exact numbers of signals and backgrounds passing cuts at selected points in the (μ, M_2) plane appear in Table 1.

Optimal choices for the numerical values given in the two cuts enumerated by bullets (•) above vary as one moves around the MSSM IP space. The specific numerical values given above were found to be quite reasonable collective compromises in simulation studies with numerous specific MSSM IP set choices. Before adopting these specific numerical values for the remainder of this work, some general remarks about the effects seen when they are varied are in order. If the missing energy cut is relaxed (or omitted), then the SM $Z^{0(*)}Z^{0(*)}$ background grows much larger. The new cut-passing $Z^{0(*)}Z^{0(*)}$ events mainly populate lines at $M_{2l} = M_Z$ on the wedgebox plot, lines thickened by the non-negligible Z^0-width. The sharp increase in the number of these background events could obscure kinematic edges due to neutralino pair-production 4ℓ signal events, *if* said edges are in the close vicinity of $M_{2l} = M_Z$. On the other hand, omission of the missing energy cut causes signal event rates to rise by roughly 20%, which may help clarify signal event kinematic edges well off the M_Z pole.

The 50 GeV threshold for identifying jets given in the jet cut is sufficient to eliminate events from gluino and squark production for squark and gluino masses down to $\sim 600\,\text{GeV}$ (note that squark and gluino IPs are fixed at 1 TeV in the remainder of this work). Tightening the jet identification threshold to 30 GeV allows elimination of events from ~ 500–$600\,\text{GeV}$ squarks and gluinos, but at the price of reducing signal rates by roughly 25%. As gluino and squark masses may not be known, it may in practice be optimal to slide this cut down to the point where

[9] The symbol "$Z^{0(*)}$" means that both on-mass-shell and off-mass-shell contributions are included.

the wedgebox plot approaches some asymptotic (direct- and Higgs-mediated-channel-dominated) shape. Note that while here the jet cut is simply based on jet energies, use of other jet observables could also be considered.

Figure 3 shows contour plots in the (μ, M_2) plane of the number of LHC events, due to the combined signal and background processes given in Fig. 2 (plus background events from slepton pair production), expected to pass the above set of cuts. An integrated luminosity of $300\,\mathrm{fb}^{-1}$ is assumed. Two 'islands' where the number of expected events exceed the 100 mark appear. Not surprisingly, rates are down (roughly by factors of from two to four) from the bounding estimates given by Fig. 2, but the general features match results from the parameter space scan. The location of the upper island fits fairly well with the locations of the maxima for direct and Higgs-mediated neutralino pair production seen in Fig. 2. In addition, according to Fig. 2, the lower island is situated where both the direct and Higgs-mediated signal processes *and* the chargino-related background processes produce substantial numbers of events. This lower island is partially contained within the LEP-excluded region. The numbers in Fig. 2 would seem to indicate that the lower island should be totally dominated by chargino-related events; however, recall that Fig. 2c does not take into account the fraction of the time the extra fifth lepton from $pp \to \widetilde{\chi}_i^0 \widetilde{\chi}_j^{\pm}$ is lost. After cuts, signal and background rates on this lower island are found to be comparable, though the chargino-related and slepton pair-production backgrounds still typically contribute a majority of the events. In particular, along a thin strip of points hugging the μ axis far from the origin, almost all events are from charged slepton pair production, which yields four leptons via a '$3+1$' process,

$$\begin{aligned} \tilde{\ell}^{\pm} &\to \ell'^{\pm} \widetilde{\chi}_2^0 \to \ell'^{\pm} \ell^{\mp} \ell^{\pm} \widetilde{\chi}_1^0 \,, \\ \tilde{\ell}^{\mp} &\to \ell'^{\mp} \widetilde{\chi}_1^0 \,. \end{aligned} \tag{6}$$

Here heavy neutralino masses kill production rates (BRs) for the direct (Higgs-mediated) neutralino pair-production modes. A corresponding strip also extends along the M_2 axis, but here sleptons prefer to decay to $\widetilde{\chi}_3^0$ until it becomes kinematically more favorable to decay to charginos ($m_{\widetilde{\chi}_3^0} > m_{\tilde{\ell}^{\pm}} > m_{\widetilde{\chi}_1^{\pm}}$) thus yielding neutrino-containing final states rather than the desired 4ℓ final state. Such '$3+1$' modes are generally characterized by a wedge with a diffuse tail extending to high invariant masses values, since one lepton pair will have a well-defined invariant mass cutoff (usually though not always $m_{\widetilde{\chi}_2^0} - m_{\widetilde{\chi}_1^0}$) while the other pair will not. For the choice of slepton masses employed herein, dominant chargino-mediated slepton decays cause the strip along the M_2 axis to terminate near $M_2 \sim 300$ GeV. The plots in Fig. 3 also illustrate that rates in the upper island region of the (μ, M_2) plane rise with $\tan\beta$. This is mainly due to increasing Higgs boson production rates – events from the Higgs-mediated channel rise from less than 10% of the total event number at $\tan\beta = 5$ to 60% at $\tan\beta = 20$ – though $\tan\beta$-induced changes in the neutralino and chargino masses and couplings also play a rôle. If the SUSY-breaking stau mass inputs are set equal to or slightly above the inputs of the first two slepton generations, then rates of all signal processes will fall precipitously after some high $\tan\beta$ limit is reached. For such high $\tan\beta$ values, mixing in the stau sector drives down one of the physical stau masses, leading to sparticle and heavy Higgs boson decays rich in tau leptons. The complex interplay of $\tan\beta$ with the observed masses and couplings underscores the difficulty in going from an observed number of events to predictions for MSSM IP values. Note however from the three plots of Fig. 3 that the gross appearance and location of the maxima where a sufficient number of events are produced is little altered.

Sneutrino spoiler modes are responsible for the drop in rates in the region between the roughly-hyperbolic dotted lines in Fig. 3 (compare with Fig. 2). The strength of these spoiler modes varies with the input slepton mass parameters chosen; these include [1] $\tan\beta$, trilinear soft A-terms whose effects are insignificant for the first two generations,

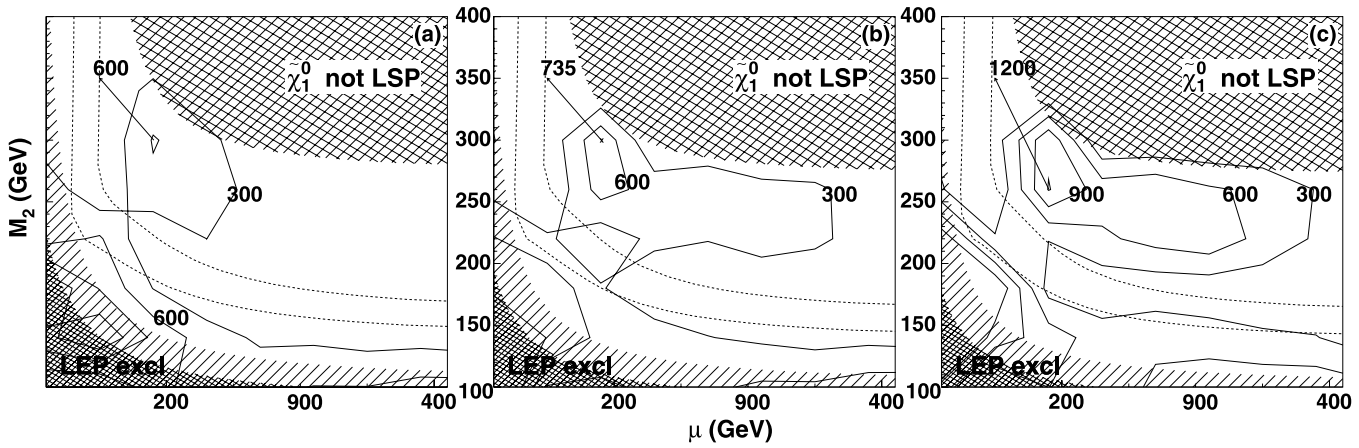

Fig. 3. Number of $e^+e^-\mu^+\mu^-$ events (event generator simulated, after cuts) at $\tan\beta = 5$ (*left*), $\tan\beta = 10$ (*middle*), and at $\tan\beta = 20$ (*right*); $m_A = 600$ GeV, $m_{\tilde{\ell}_{\mathrm{L}}} = m_{\tilde{\ell}_{\mathrm{R}}} = 150$ GeV ($\ell = e, \mu$) and $m_{\tilde{\tau}} = 250$ GeV. Assuming an integrated luminosity of $300\,\mathrm{fb}^{-1}$. The region between the two hyperbolic dashed curves is where the sneutrino spoiler modes cut heavily into event rates

and the soft slepton mass inputs. Results with the canonical choice of $m_{\tilde{\ell}_{\rm L}} = m_{\tilde{\ell}_{\rm R}} = 150\,\text{GeV}$ (used in all of the other figures presented in this work) seen in the center ($\tan\beta = 10$) plot of Fig. 3 may be compared to those from elevating $m_{\tilde{\ell}_{\rm L}}$ to 200 GeV in Fig. 4. Elevating $m_{\tilde{\ell}_{\rm L}}$ raises the physical sneutrino masses (as well as the masses of the left charged sleptons) above those of the right charged sleptons, shutting down the spoiler modes. Comparing the two results, we see that the rates when $m_{\tilde{\ell}_{\rm L}}$ is made heavier actually increase despite the diminution of the left charged slepton channel. The ravine of low event rates that cuts across the plots in Fig. 3 has mostly vanished. A third maximum also now appears near $(\mu, M_2) = (390\,\text{GeV}, 180\,\text{GeV})$. It is almost completely due to Higgs-mediated $H^0/A^0 \to \widetilde{\chi}^0_2\widetilde{\chi}^0_{2,3}$ modes (cross-sections for direct modes are too small here). As one moves off this peak to lower M_2 or μ, intermediate sleptons become off-shell and suppress $\widetilde{\chi}^0_2 \to \ell^+\ell^-\widetilde{\chi}^0_1$ decays, whereas moving to higher values of these parameters raises the masses of $\widetilde{\chi}^0_{2,3}$ and thus suppresses $H^0/A^0 \to \widetilde{\chi}^0_2\widetilde{\chi}^0_{2,3}$ modes.

The foregoing analysis demonstrates that over a very broad range of values for $\tan\beta$, M_A, and the slepton masses,[10] there are always two disjoint regions of high (over 300 events per $300\,\text{fb}^{-1}$) rates in the (μ, M_2) plane. Next the topological variation of the wedgebox plot patterns obtained at different IP space points across these high-event regions will be investigated. Taking for definiteness $\tan\beta = 20$ (right plot of Fig. 3), wedgebox plots are generated at an array of (μ, M_2) points, assuming an integrated luminosity of $300\,\text{fb}^{-1}$, to obtain the 'wedgebox map' shown in Fig. 5. Each symbol in the wedgebox map represents a shape ascertained from visual inspection of the corresponding wedgebox plot (explicit examples are forthcoming) at that point. This wedgebox map represents the potential of the LHC to correlate neutralino MSSM IPs μ and M_2 with an observed wedgebox shape if nature has chosen $\tan\beta = 20$, $M_A = 600\,\text{GeV}$, $m_{\tilde{g},\tilde{q}} = 1000\,\text{GeV}$, and $m_{\tilde{\ell}_{\text{L,R}\,i}} = 150\,\text{GeV}$ $(i = e, \mu)$, 250 GeV $(i = \tau)$. Figure 5 is thus a representative example of a class of (μ, M_2) wedgebox plots that can be made by varying these additional inputs.

Toward the lower-left-hand corner of Fig. 5, in the region of the lower island, one sees a fairly complicated evolution of shapes, as might be expected since here the direct, Higgs-mediated, chargino-related and slepton pair production modes all contribute significantly. For example, the wedgebox pattern for the point $(\mu, M_2) = (150\,\text{GeV}, 160\,\text{GeV})$ is depicted in Fig. 5 as a box with a wedge extending out of it. The actual wedgebox plot is shown in Fig. 6a (see Table 1 for a breakdown of events passing cuts). A sizable fraction of the events are chargino-related mavericks (as discussed in Sect. 1). While some kinematical edges are clearly visible, the high fraction of mavericks makes it sometimes challenging to connect these with mass differences in the neutralino spectrum. For example, the clustering of points near 45 GeV is in fact

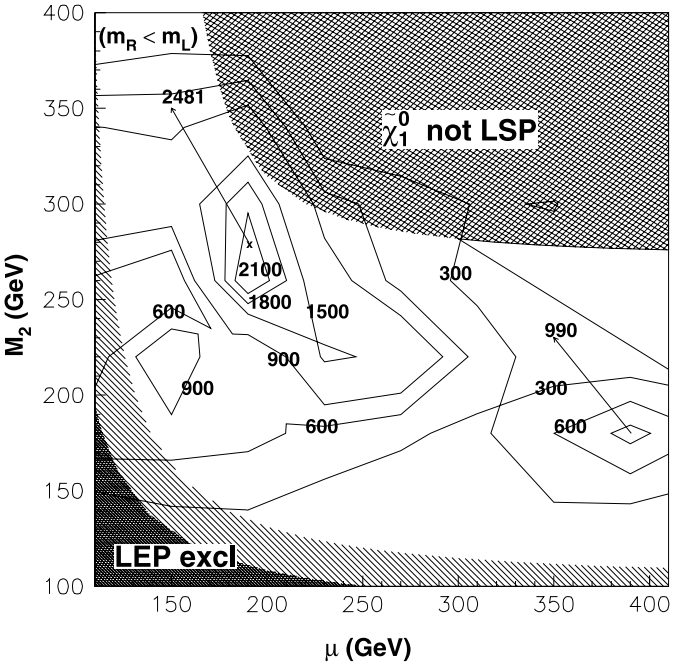

Fig. 4. Number of $e^+e^-\mu^+\mu^-$ events (event generator simulated, after cuts) with $\tan\beta = 10$, $m_{\tilde{\ell}_{\rm L}} = 200\,\text{GeV}$ and $m_{\tilde{\ell}_{\rm R}} = 150\,\text{GeV}$ $(\ell = e, \mu)$ and $m_{\tilde{\tau}} = 250\,\text{GeV}$; $m_A = 600\,\text{GeV}$. Assuming an integrated luminosity of $300\,\text{fb}^{-1}$

a mixture of the $\widetilde{\chi}^0_2 \to \widetilde{\chi}^0_1$ decay edge through an off-shell slepton (readily calculable from Table 2: $M_{21}(\ell^+\ell^-) = 45.7\,\text{GeV}$) and the $\widetilde{\chi}^0_3 \to \widetilde{\chi}^0_1$ edge through on-shell sleptons $(32.5\,\text{GeV} < M_{31}(\ell^+\ell^-) < 45.5\,\text{GeV})$.[11] The large width of M_{31} here is due to the proximity of the slepton masses to that of $\widetilde{\chi}^0_3$. Moreover, the edge seen near 115 GeV arises not from a neutralino decay, but from $\widetilde{\chi}^\pm_2 \to \widetilde{\nu}\ell^\pm \to \widetilde{\chi}^\pm_1\ell^\pm\ell^\mp$: this decay yields two leptons with an invariant mass cutoff of 118.7 GeV determined by the charginos' mass difference. Not easily discernible in the plot is another edge from $\widetilde{\chi}^0_4 \to \widetilde{\chi}^0_1$ decays (calculated as $141.8\,\text{GeV} < M_{41}(\ell^+\ell^-) < 144.6\,\text{GeV}$); these mostly come from Higgs-mediated events. Finally, for small values of M_{ee} and/or $M_{\mu\mu}$ along the axes there are long tails, which gradually taper off. A wedge with diffuse tails extending to high invariant mass values is the hallmark of '$3+1$' decay modes as in (6). Most of these events result from slepton pair production. The multitude of significant

[10] Assuming these are less than $\sim 300\,\text{GeV}$, otherwise event rates are too low.

[11] Here it is necessary to make note of a small inadequacy in the analysis package used to generate the wedgebox plots: a term in the slepton masses from left-right sfermion mixing – the $m_\ell^2\mu^2\tan^2\beta$ term in (13) of [1] – is neglected in ISASUSY 7.58 [11, 12] which feeds the mass values into HERWIG 6.5 [16, 17]. Neglecting this term, the mass splitting of the smuons becomes equal to that of the selectrons, and thus is evidently sometimes underestimated. Numerical values given in the text correctly account for this term and so may not exactly correspond to what is observed in the wedgebox plot figures, though the differences are not crucial to the current analysis and discussion.

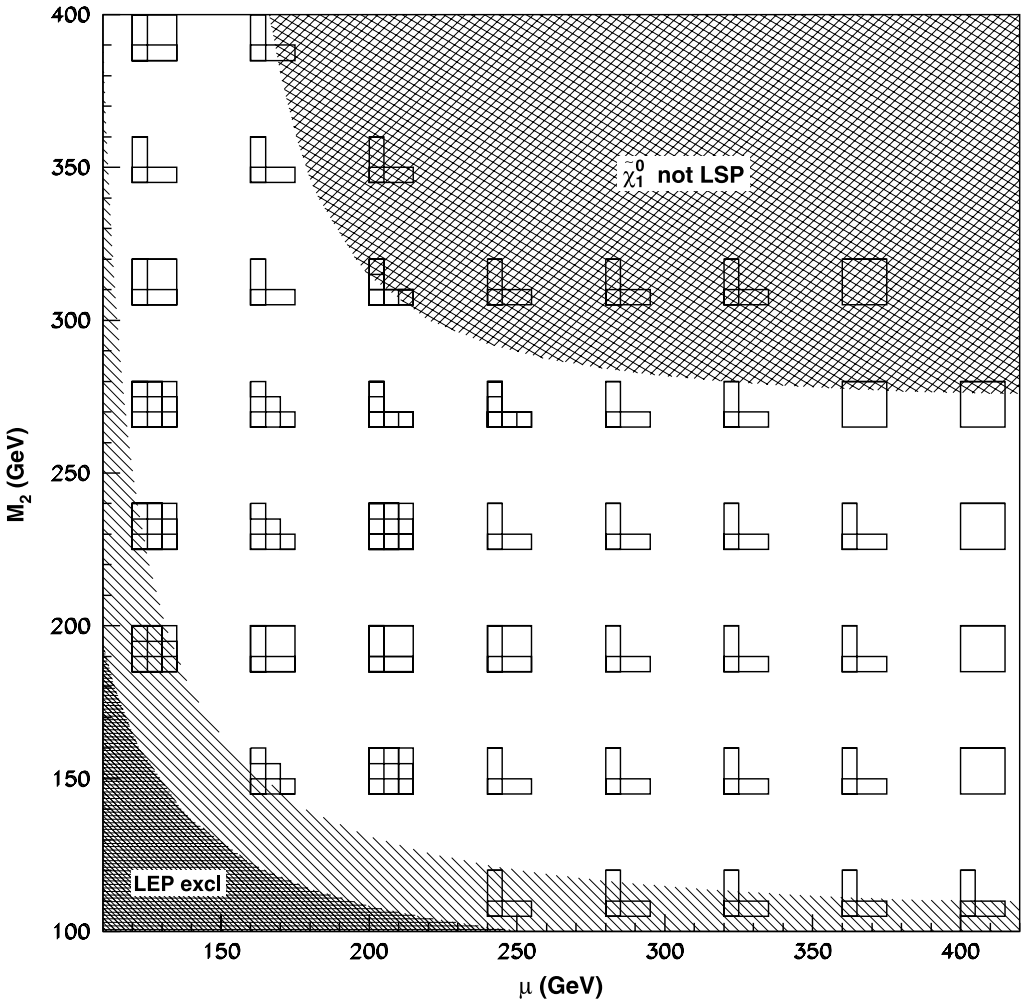

Fig. 5. Wedgebox 'map' for $\tan\beta = 20$ and assuming an integrated luminosity of $300\,\mathrm{fb}^{-1}$. Idealized wedgebox plot patterns abstracted from visual inspections of wedgebox plots obtained from simulation runs at an array of points spanning the parameter space. Values of other fixed parameters: $m_A = 600\,\mathrm{GeV}$, $m_{\tilde{g},\tilde{q}} = 1000\,\mathrm{GeV}$, and $m_{\widetilde{\ell}_{\mathrm{L,R}\,i}} = 150\,\mathrm{GeV}$ $(i = e,\mu)$, $250\,\mathrm{GeV}$ $(i = \tau)$. The uncertainty shown in the extent of the LEP excluded region stems from the presence of a relatively light sneutrino (as discussed in an earlier footnote)

Table 2. Neutralino masses at the representative points $(\mu, M_2) = (150, 160)$ and $(\mu, M_2) = (190, 280)$ (all masses in GeV), as well as expected average values of kinematic endpoints

	$(150, 160)$	$(190, 280)$
$\widetilde{\chi}_1^0$	67.1	122.3
$\widetilde{\chi}_2^0$	112.8	180.8
$\widetilde{\chi}_3^0$	163.2	198.8
$\widetilde{\chi}_4^0$	223.2	315.8
M_{21}	45.7	56.8
M_{31}	39.0	76.9
M_{41}	143.2	172.2

source processes for the event points, the quick evolution of wedgebox patterns as one moves around the (μ, M_2) plane, and the strong contingent of maverick events all make this a tricky region of the MSSM IP space to analyze via the methodology adopted here. On the other hand, a sufficiently complicated wedgebox plot may indicate that nature has chosen a point in this relatively small (especially given the portion ruled out by LEP) sector of the IP space.

As one moves to higher values of μ and M_2, the wedgebox shapes become much less sensitive to small shifts in the (μ, M_2) plane. In the region of the upper island the wedgebox pattern almost exclusively consists of either a wedge, a 'double-wedge', or a box. This is primarily because the chargino-related production modes are far weaker in this region, and thus the dominant source of events is direct neutralino pair production, which as stated earlier is basically just $\widetilde{\chi}_2^0\widetilde{\chi}_3^0$ production, along with Higgs-mediated neutralino pair production. In fact at sufficiently high values of M_2 or μ only this latter contributes via $H^0/A^0 \to \widetilde{\chi}_2^0\widetilde{\chi}_2^0$, giving a simple box shape. In the interior of the upper island direct $\widetilde{\chi}_2^0\widetilde{\chi}_3^0$ production yields one wedge with an inner (outer) edge at $M_{i1}(\ell^+\ell^-)$ for $i = 2(3)$. Significant Higgs-mediated modes in this region are $H^0/A^0 \to \widetilde{\chi}_2^0\widetilde{\chi}_2^0$, $\widetilde{\chi}_2^0\widetilde{\chi}_3^0$ and $\widetilde{\chi}_2^0\widetilde{\chi}_4^0$. However, for most points on the upper island the crucial $\widetilde{\chi}_2^0\widetilde{\chi}_4^0$ contribution is too faint to give a distinct edge, and the other Higgs processes will simply reinforce the kinematical edges[12] from $\widetilde{\chi}_2^0\widetilde{\chi}_3^0$ production, yielding a single wedge. An exception to this rule occurs near the maximum of the island at

[12] Though the population structure within elements of the wedgebox plot will be altered.

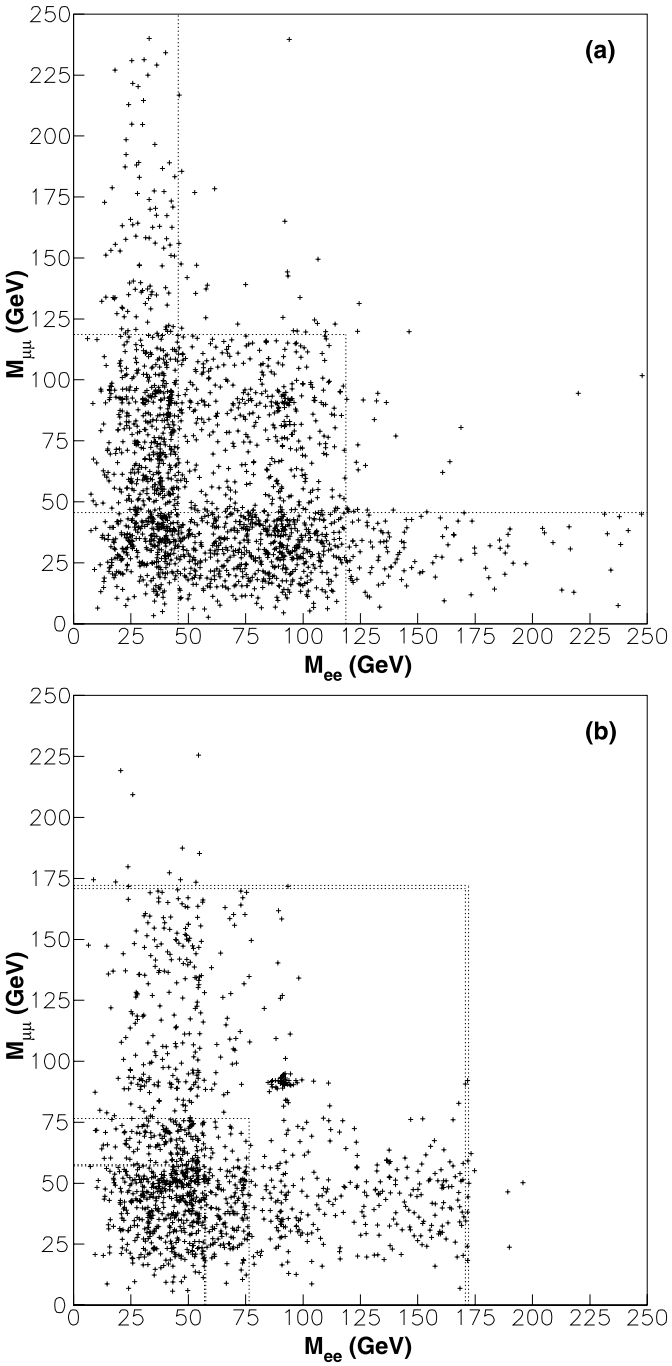

Fig. 6. Wedgebox patterns for an integrated luminosity of $300\,\mathrm{fb}^{-1}$ at **a** $(\mu, M_2) = (150\,\mathrm{GeV}, 160\,\mathrm{GeV})$ and **b** $(\mu, M_2) = (190\,\mathrm{GeV}, 280\,\mathrm{GeV})$; in both cases $\tan\beta = 20$, $m_A = 600\,\mathrm{GeV}$, and $m_{\tilde{\ell}_\mathrm{L}} = m_{\tilde{\ell}_\mathrm{R}} = 150\,\mathrm{GeV}$. *Dashed lines* indicate expected positions of kinematic endpoints (see Table 2 for specific numbers). All backgrounds remaining after cuts as described in the text are included. The bin size is 2.5 GeV along each axis. The HERWIG [16, 17] event generator was used

$(M_2, \mu) = (190\,\mathrm{GeV}, 280\,\mathrm{GeV})$ where the $\widetilde{\chi}_2^0\widetilde{\chi}_4^0$ contribution is substantial and a second wedge extends out from the first with an inner (outer) edge at $M_{i1}(\ell^+\ell^-)$ for $i = 2(4)$, giving a 'double wedge'.

In the special region where a double-wedge pattern is observed, one can unambiguously identify the quantities $M_{i1}(\ell^+\ell^-)$ $(i = 2, 3, 4)$ which will put very significant constraints on the neutralino and physical slepton masses; these in turn determine the MSSM IPs M_1, M_2, μ, $\tan\beta$ and $m_{\tilde{e}_\mathrm{L,R}}$, $m_{\tilde{\mu}_\mathrm{L,R}}$. Figure 6b shows the MC simulation of the double wedge at $(\mu, M_2) = (190\,\mathrm{GeV}, 280\,\mathrm{GeV})$, assuming an integrated luminosity of $300\,\mathrm{fb}^{-1}$. As both direct and Higgs-mediated modes contribute over 1000 events each at this point (triple the numbers in Table 1), the approximate locations of the three kinematic edges are easily visible. Unfortunately, as a practical matter high rates such as these are indispensable in comfortably distinguishing a double wedge from a single wedge. In fact, there is no definitive division between the two wedgebox shapes: quantitative criteria must be developed to gauge how many events are required to adequately resolve the outer edge of the longer wedge. Here visual inspection certainly indicates that $300\,\mathrm{fb}^{-1}$ of integrated luminosity suffices at this point in IP space, with $M_{21}(\ell^+\ell^-) = 55 \pm 5\,\mathrm{GeV}$, $M_{31}(\ell^+\ell^-) = 75 \pm 5\,\mathrm{GeV}$, and $M_{41}(\ell^+\ell^-) = 175 \pm 10\,\mathrm{GeV}$. Since here points are generated by a MC event simulator, one of course knows the actual values for these edges: $M_{21}(\ell^+\ell^-) = 56.9\,\mathrm{GeV}$, $M_{31}(\ell^+\ell^-) = 76.8\,\mathrm{GeV}$, $M_{41}(\ell^+\ell^-) = 171.7\,\mathrm{GeV}$ on the muon side, and $M_{21}(\ell^+\ell^-) = 56.6\,\mathrm{GeV}$, $M_{31}(\ell^+\ell^-) = 76.9\,\mathrm{GeV}$, $M_{41}(\ell^+\ell^-) = 172.6\,\mathrm{GeV}$ on the electron side.[13] Clearly observations from the wedgebox plot and the values calculated from the known MSSM IPs are in reasonable agreement. The uncertainties given above are simply eye-ball estimates that may of course be more carefully studied utilizing statistical likelihood methodologies; however, it is already abundantly clear that the two-dimensional wedgebox plot offers a more precise method of edge identification than the traditional one-dimensional projection. One can, for instance, see shifts between the edge locations along the two axes (perhaps indicating slepton mass non-degeneracy for instance) in what would, in a one-dimensional plot, be taken as just one broader edge. One can also discard some of the maverick events that fall outside the regular structures of the wedgebox plot – for instance points in the regions $(M_{ee}, M_{\mu\mu}) = (125$–$175\,\mathrm{GeV}, 50$–$90\,\mathrm{GeV})$ and $(50$–$90\,\mathrm{GeV}, 125$–$175\,\mathrm{GeV})$ in Fig. 6a. Further, anomalies in the population densities of structures presumed to be mirror images of each other along the two axes may become apparent.

Though sub-dominant, a significant number of the events at points on the upper island still do arise from chargino production. For a quantitative estimate, a random sampling of non-Higgs-mediated events passing all cuts near the maximum of the second island was examined: 75% of these were direct neutralino production $\widetilde{\chi}_2^0\widetilde{\chi}_3^0$ events yielding the expected inner wedge, while almost all the remaining events involved chargino production. Ap-

[13] This slight asymmetry arises from differences in the physical selectron and smuon masses which are due only to the fact that $m_\mu \neq m_e$ – here $m_{\tilde{\mu}_\mathrm{L,R}}$ and $m_{\tilde{e}_\mathrm{L,R}}$ remain degenerate. See earlier comments though concerning the event generator.

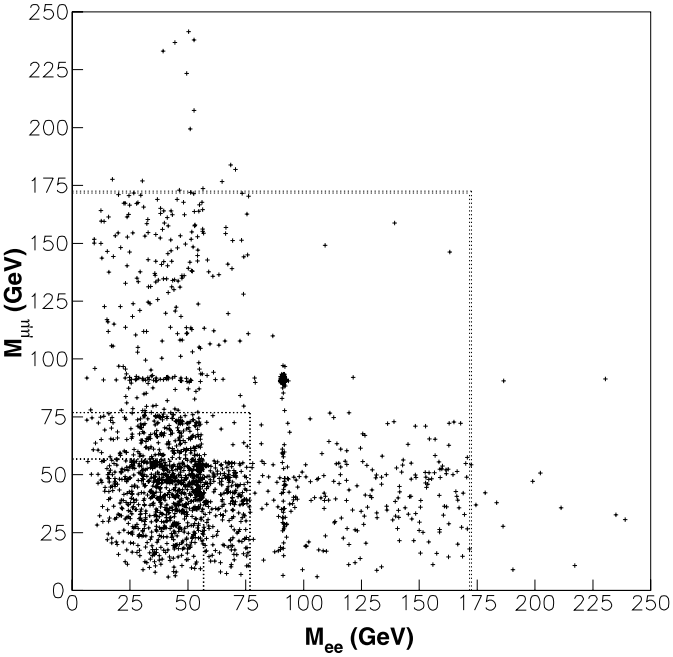

Fig. 7. The wedgebox plot at $(\mu, M_2) = (190\,\text{GeV}, 280\,\text{GeV})$ and $\tan\beta = 20$, assuming an integrated luminosity of $300\,\text{fb}^{-1}$. This plot was made using ISAJET [11, 12]; compare to Fig. 6b, made using HERWIG

proximately half of the chargino events are '$3+1$' events from chargino pair production, either $\widetilde{\chi}_2^{\pm}\widetilde{\chi}_1^{\mp}$ or $\widetilde{\chi}_2^{\pm}\widetilde{\chi}_2^{\mp}$. The chargino yielding three leptons either decays via $\widetilde{\chi}_2^{\pm} \to \widetilde{\chi}_2^0 W^{\pm}$ (with the $W^{\pm}$ decaying leptonically), reinforcing the edges of the box in the lower-left corner of the wedgebox plot, or via $\widetilde{\chi}_2^{\pm} \to Z^0\widetilde{\chi}_1^{\pm}$, leading to Z-lines on the wedgebox plot. The lighter chargino, $\widetilde{\chi}_1^{\pm}$, decays over 90% of the time into a sneutrino and a single lepton, and the remaining $< 10\%$ of the time into a charged slepton and a neutrino, again yielding exactly one lepton. Almost all the remaining chargino events were from $\widetilde{\chi}_2^{\pm}\widetilde{\chi}_{2,4}^0$ chargino–neutralino production. Here the $\widetilde{\chi}_2^{\pm}$ decays via $\widetilde{\chi}_2^{\pm} \to \widetilde{\chi}_2^0 W^{\pm}$, with the $W^{\pm}$ decaying hadronically yet not leading to jets strong enough to violate the jet cut. In summary, events involving charginos are present in significant numbers, but they add no new edges (save possibly Z-lines) to the wedgebox plot.

Figure 7 again shows the wedgebox plot for $(\mu, M_2) = (190\,\text{GeV}, 280\,\text{GeV})$ and $\tan\beta = 20$, assuming an integrated luminosity of $300\,\text{fb}^{-1}$, as in Fig. 6b. The difference is that Fig. 7 uses the ISAJET 7.64 [11, 12] event generator, while Fig. 6b utilizes the HERWIG 6.5 [16, 17] Monte Carlo package (in both cases, the CTEQ 6M [18, 19] set of structure functions is used, while different but comparable detector simulation programs are employed). While the exact number and placements of events do not coincide, the over-all topologies seen in the two plots are virtually identical. Using ISAJET facilities for separating out the contributions from each production process yields the plots shown in Fig. 8, and the corresponding numbers of events per catagory detailed in Table 3. In Fig. 8, the upper left plot a is only from direct $\widetilde{\chi}_2^0\widetilde{\chi}_3^0$ production, while

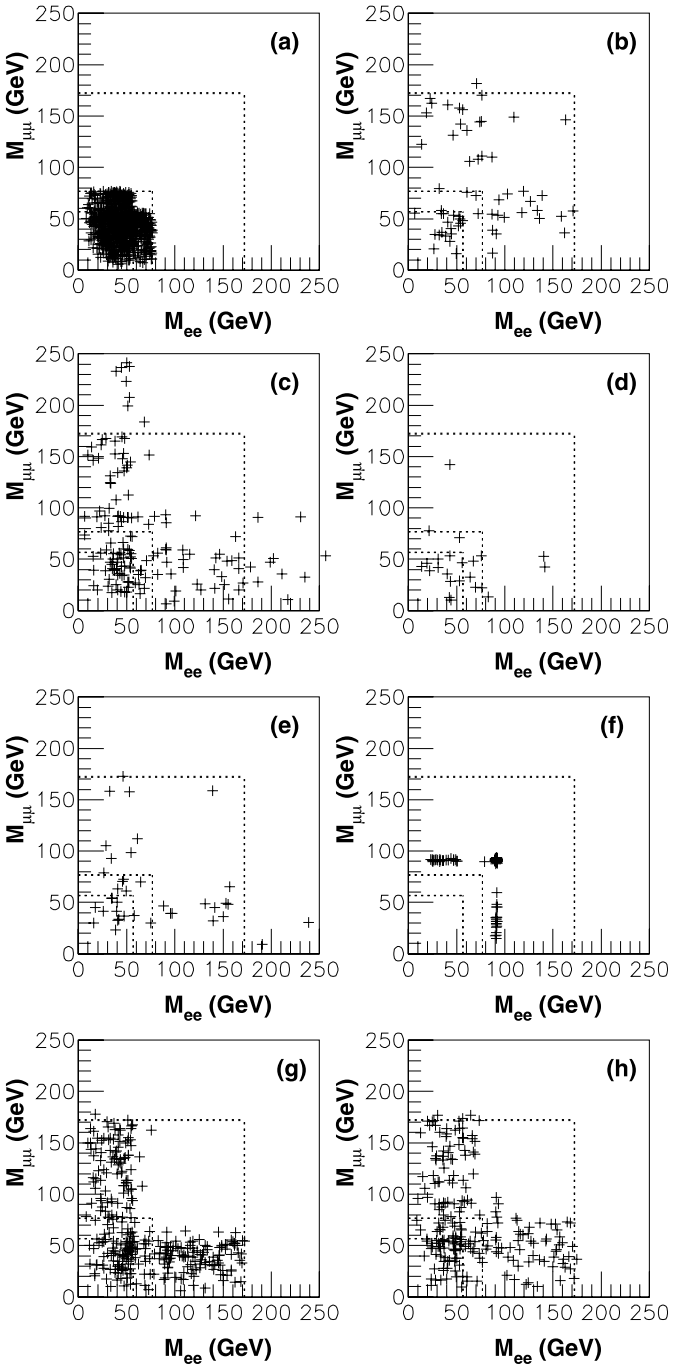

Fig. 8. The wedgebox plot at $(\mu, M_2) = (190\,\text{GeV}, 280\,\text{GeV})$ (with $\tan\beta = 20$ and for $300\,\text{fb}^{-1}$) broken down into contributions from **a** $\widetilde{\chi}_2^0\widetilde{\chi}_3^0$; **b** other $\widetilde{\chi}_i^0\widetilde{\chi}_j^0$ combinations; **c** $\widetilde{\chi}_i^{\pm}\widetilde{\chi}_j^{\mp} + \widetilde{\chi}_i^{\pm}\widetilde{\chi}_j^{\pm} + \widetilde{\chi}_i^{\pm}\widetilde{\chi}_i^0$; **d** direct slepton production; **e** $tH^- + \bar{t}H^+$; **f** $Z^0Z^{0(*)}$; **g** A^0; and **h** H^0. Combining the $\widetilde{\chi}_2^0\widetilde{\chi}_3^0$ and A^0, H^0 components yields the double-wedge wedgebox plot (augmented by a halo from the chargino and $tH^-, \bar{t}H^+$ components and by Z-lines) of Fig. 7. Analysis done using ISAJET [11, 12]

the lower plots g and h are from A^0 and H^0 production, respectively; together, these form the double-wedge topological structure apparent in Fig. 7. Note from the dashed lines at the expected endpoints (from Table 2) how well

Table 3. Separate contributions of different processes at the MSSM parameter space point $(\mu, M_2) = (190\,\text{GeV}, 280\,\text{GeV})$, assuming an integrated luminosity of $300\,\text{fb}^{-1}$. Results based on ISAJET [11, 12] simulations (including the tH^-, $\bar{t}H^+$ processes, which rely on added non-public code), except for the $t\bar{t}h^0$ and $t\bar{t}Z^{0(*)}$ processes, for which HERWIG results are used

Process	tot. evts.†	$e^+e^-\mu^+\mu^-$ evts.	evts. pass cuts
A^0	199 020	665	318
H^0	196 980	499	218
$\widetilde{\chi}_2^0\widetilde{\chi}_2^0$	167	25	11
$\widetilde{\chi}_2^0\widetilde{\chi}_3^0$	40 620	1539	888
$\widetilde{\chi}_2^0\widetilde{\chi}_4^0$	475	29	6
$\widetilde{\chi}_3^0\widetilde{\chi}_3^0$	31	0	0
$\widetilde{\chi}_3^0\widetilde{\chi}_4^0$	4854	79	41
$\widetilde{\chi}_4^0\widetilde{\chi}_4^0$	428	8	3
$\widetilde{\chi}_1^0\widetilde{\chi}_{2,3,4}^0$	41 322	0	0
$\widetilde{\chi}_1^+\widetilde{\chi}_1^-, \widetilde{\chi}_1^\pm\widetilde{\chi}_1^\pm$	168 390	0	0
$\widetilde{\chi}_1^\pm\widetilde{\chi}_2^\mp, \widetilde{\chi}_1^\pm\widetilde{\chi}_2^\pm$	5117	14	7
$\widetilde{\chi}_2^+\widetilde{\chi}_2^-, \widetilde{\chi}_2^\pm\widetilde{\chi}_2^\pm$	31 080	241	73
$\widetilde{\chi}_{1,2}^\pm\widetilde{\chi}_1^0$	147 960	0	0
$\widetilde{\chi}_1^\pm\widetilde{\chi}_{2,3,4}^0$	323 220	2	1
$\widetilde{\chi}_2^\pm\widetilde{\chi}_{2,3,4}^0$	53 163	355	76
sleptons	242 550	77	23
$\tilde{g}\tilde{g}$, $\tilde{g}\tilde{q}$, $\tilde{q}\tilde{q}$	375 900	3480	0
$\tilde{g}\widetilde{\chi}_i^0$, $\tilde{q}\widetilde{\chi}_i^0$, $\tilde{g}\widetilde{\chi}_j^\pm$, $\tilde{q}\widetilde{\chi}_j^\pm$	40 581	408	3
tH^-, $\bar{t}H^+$	43 554	242	40
$t\bar{t}h^0$	143 677	3	0
$t\bar{t}Z^{0(*)}$	130 560	38	3
$Z^0Z^{0(*)}$	2 514 000	2287	288

† A threshold p_T of 20 GeV was required for initial particles produced in 2-body production processes and for inital decay products from Higgs boson production.

the direct $\widetilde{\chi}_2^0\widetilde{\chi}_3^0$, A^0 and H^0 events conform to the theoretical expectations:[14] $\widetilde{\chi}_2^0\widetilde{\chi}_3^0$ production yields a clean, relatively short, wedge with an outer edge at ~ 80 GeV, and H^0, A^0 production gives a longer $(\widetilde{\chi}_2^0\widetilde{\chi}_4^0)$ wedge terminating around 175–180 GeV. Also marginally discernible in the A^0 (H^0) plot is a population change around 55–60 GeV (75–80 GeV) corresponding to $\widetilde{\chi}_2^0\widetilde{\chi}_2^0$ $(\widetilde{\chi}_2^0\widetilde{\chi}_3^0)$ decays of the Higgs boson. 'Maverick' ('3 + 1') chargino events and to a lesser extent $tH^-, \bar{t}H^+$ production produce the halo events that fall outside of the expected signal event zones demarcated by the dashed lines, and $Z^0Z^{0(*)}$ (and $t\bar{t}Z^0$) production, with some augmentation from chargino events, adds Z-lines.[15] While contributions from other $\widetilde{\chi}_i^0\widetilde{\chi}_j^0$ direct production modes (plot b in Fig. 8), from chargino-containing production processes (plot c) and from direct slepton production (plot d) are certainly not structureless, the edges (vaguely) visible from these contributions merely reinforce the edges seen in the A^0, H^0 and direct $\widetilde{\chi}_2^0\widetilde{\chi}_3^0$ plots, and the halo events and Z-line events from these and other processes do not prevent one from identifying the $\widetilde{\chi}_2^0\widetilde{\chi}_3^0$ and H^0, A^0 edges. This is true of all the upper island wedgebox plots examined: the maverick event characteristics do not obscure identification of the sought-after neutralino-based endpoints. The chargino-derived Z-line events do sometimes make the overall wedgebox plot look fatter, and one must be cautious not to be misled by mavericks which partially fill in the space between the Z-lines and the wedges. Increased luminosity will help clarify any uncertainty here.

Figure 5 is a representative example of a class of (μ, M_2) wedgebox plots for one set of m_A, $\tan\beta$ and slepton inputs. If the $\tan\beta$ value is lowered from $\tan\beta = 20$, the total rate drops as seen in Fig. 3. However, for $5 < \tan\beta < 20$, the '100' event contour still covers nearly the whole region of Fig. 5, so enough events may be collected to build a respectable wedgebox plot. Since it is really the Higgs boson processes which are losing rate while other processes are roughly constant, on the lower island diminishing the already minor Higgs boson contribution does not markedly affect the already complicated chargino-dominated wedgebox structure while on the upper island removing the Higgs contribution at worst removes the edge associated with $H/A \to \widetilde{\chi}_2^0\widetilde{\chi}_4^0$ (since $H^0/A^0 \to \widetilde{\chi}_2^0\widetilde{\chi}_{2,3}^0$ simply reinforce edges already present from direct and chargino channels). So for lower $\tan\beta$ values, it may not be possible to observe the double wedge: somewhere between $\tan\beta = 10$ (Fig. 8) and $\tan\beta = 20$ (Fig. 6b) the number of events seen at $(\mu, M_2) = (190\,\text{GeV}, 280\,\text{GeV})$ drops below '300' for $300\,\text{fb}^{-1}$, making it more difficult to cleanly identify the $M_{41}(\ell^+\ell^-)$ edge of the outer wedge of the double wedge. Thus analogous plots to Fig. 5 for $\tan\beta$ values of 5 or 10 look quite similar to Fig. 5 save that more and more double-wedge wedgebox plots will become simple single-wedge wedgebox plots. As $\tan\beta$ rises above 20, rates may continue to rise – if SUSY-breaking stau mass inputs are set safely above the corresponding selectron and smuon inputs, as has been done by hand here – or they may plummet (as noted earlier) – if stau inputs are made degenerate with those of the first two generations, in which case mixing will increasingly drive down one of the physical stau masses as $\tan\beta$ grows, cutting down 'leptonic' (that is, electron and muon) BRs in favor of decays yielding taus.

The preceding paragraph touched upon the dependence of the appearance of Fig. 5 on inputs of the slepton sector, specifically, the value(s) of the stau inputs relative to those of the first two generations. Now, setting aside the staus for the moment, consider how changing the selectron and smuon inputs will affect results. If the first two generations' degenerate input mass is raised above (lowered below) the nominal value of 150 GeV assumed in Fig. 5, all rates decline (grow). Repeating here the rough estimates given above, if rates fall significantly below 300 events per

[14] A few events do stray very slightly over the M_{41} endpoints along the high $M_{\mu\mu}$ side in the $\widetilde{\chi}_i^0\widetilde{\chi}_j^0$, A^0 and H^0 plots. This is due to the muon energy/momentum smearing in the detector.

[15] More Z^0Z^0 events pass the cuts in the ISAJET-based analysis than in the HERWIG-based one; however, as these events fall along the Z-lines, this does not affect the determination of the wedgebox topology.

$300\,\mathrm{fb}^{-1}$ at an upper island point in the MSSM IP space, double-wedge wedgebox plots tend to become single-wedge wedgebox plots, and if rates drop much below 100 events per $300\,\mathrm{fb}^{-1}$, no clear wedgebox pattern may emerge at all. Thus by merely determining the overall event rate at a point and then referencing Fig. 5, a good estimate of what the wedgebox plot at that point should look like can often be deduced. If the degeneracy of the slepton mass inputs is lifted, then rates can be raised even if the left slepton inputs are made more massive, since as mentioned previously the sneutrino masses will rise and suppress the spoiler modes (see Fig. 4). If smuon SUSY-breaking mass inputs are pushed above those of the selectrons (or vice versa) rates drop as the $e^+e^-e^+e^-$ event rate grows at the expense of the $e^+e^-\mu^+\mu^-$ and $\mu^+\mu^-\mu^+\mu^-$ event rates.[16]

Lastly, consider the impact of altering m_A. This would affect the Higgs boson contributions (the focus of [2, 3]) to the wedgebox plot. If m_A is lowered significantly, then the only open Higgs decay channel to neutralinos would be to $\widetilde{\chi}_2^0\widetilde{\chi}_2^0$. This would produce a $\widetilde{\chi}_2^0\widetilde{\chi}_2^0$ box. If direct $\widetilde{\chi}_2^0\widetilde{\chi}_3^0$ production is significant, then the Higgs boson-induced $\widetilde{\chi}_2^0\widetilde{\chi}_2^0$ box would lie at the corner of the $\widetilde{\chi}_2^0\widetilde{\chi}_3^0$ wedge, producing no new edges and thus indistinguishable *by shape* from a wedgebox plot consisting solely of a $\widetilde{\chi}_2^0\widetilde{\chi}_3^0$ wedge. However, the presence of the Higgs boson-induced $\widetilde{\chi}_2^0\widetilde{\chi}_2^0$ box may well be noticeable via the population structure of the various component parts of the wedge – the Higgs boson decays in this case will overpopulate the corner box of the wedge. The Higgs boson is critical to producing the very desirable double-wedge pattern, and, to allow this, m_A must be large enough to allow H^0 and[17] A^0 to decay to $\widetilde{\chi}_2^0\widetilde{\chi}_4^0$. Yet if m_A is made too large, Higgs boson production rates drop off and the Higgs boson contribution dies.

4 Discussion

Figure 9 shows the conventional one-dimensional projections which may be obtained from the two wedgebox plots in Fig. 6 by plotting both the $M(e^+e^-)$ and the $M(\mu^+\mu^-)$ values from each event along a single axis. While mass differences may still be inferred from sharp changes in curvature,[18] information gained from correlating the $M(e^+e^-)$ and $M(\mu^+\mu^-)$ values is clearly lost, meaning that whether the events are generated chiefly by similar or dissimilar neutralino pair production may no longer be determined. Further, the ability to identify and thus exclude so-called 'maverick' events outside of the wedge and box geometrical elements of the two-dimensional wedgebox plot is lost, and so one means of further purifying the data sample and perhaps better resolving the kinematical edges is also lost.

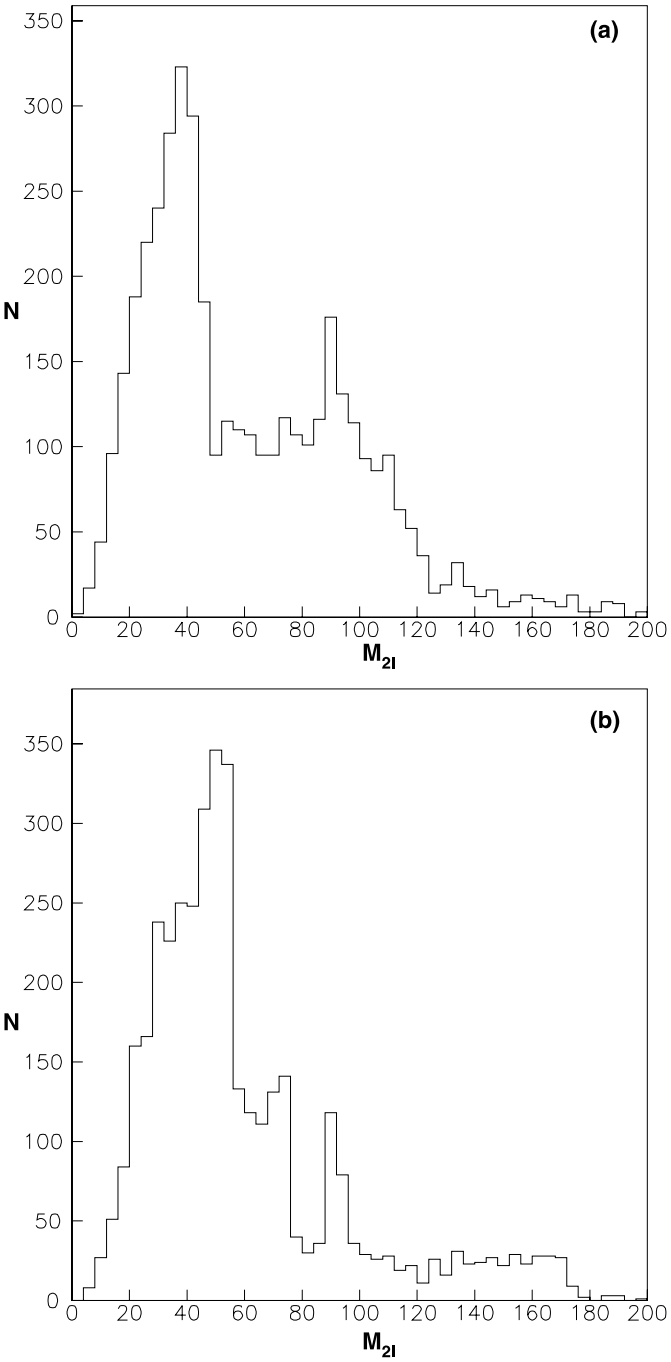

Fig. 9. One-dimensional projections of the two wedgebox plots in Fig. 6 obtained by putting values of both $M(e^+e^-)$ and $M(\mu^+\mu^-)$ for each event on one axis

Two-dimensional wedgebox plots contain considerably more information often packaged in a readily understandable manner. For instance, a double-wedge or wedge-protruding-from-a-box wedgebox plot almost always[19] has

[16] This could be dealt with if $e^+e^-e^+e^-$ event-types can be utilized as well [15].

[17] For larger values of m_A relevant here, H^0 and A^0 are nearly degenerate.

[18] Though care must be taken in interpreting, for instance, the maverick-induced glitch near 60 GeV in the upper plot or rate increases around the Z^0 pole in both plots.

[19] This general rule can be broken by $\widetilde{\chi}_2^\pm \to \widetilde{\chi}_1^\pm \ell^+\ell^-$ decay events or by so-called 'stripes' [1], where $\widetilde{\chi}_i^0 \to \widetilde{\chi}_j^0 \ell^+\ell^-$ $(j \neq 1)$. The former was mainly encountered in the region of the lower island and the latter was never found to be significant.

edges corresponding to $\widetilde{\chi}_i^0 \to \widetilde{\chi}_1^0$ decays ($i = 2, 3, 4$ in order of proceeding out along either axis). The numerical values for the locations of these edges will either be the $m_{\widetilde{\chi}_i^0} - m_{\widetilde{\chi}_1^0}$ mass difference or[20] a well-defined function of $m_{\widetilde{\chi}_i^0}$, $m_{\widetilde{\chi}_1^0}$ and slepton masses, that is, (4); both possibilities allow for the extraction of substantial information on the MSSM neutralino mixing matrix and perhaps the slepton sector. Technically, in other wedgebox patterns with fewer edges there is an inherent ambiguity in identifying the $\widetilde{\chi}_i^0 \to \widetilde{\chi}_1^0$ decay responsible for each edge, though in practice taking the lowest available i for each edge is usually the correct choice; and the information concerning the MSSM input parameters extractable remains quite significant.

Since large integrated luminosities (probably over $100\,\mathrm{fb}^{-1}$) are typically required to make a clear wedgebox plot, probably several years of LHC running will be necessary before meaningful results are obtainable. Prior to this, other techniques involving invariant masses [4, 27–32] may well have provided information on gluino and squark masses, m_h, and the lowest-lying masses, or mass-differences, among the EW sparticles.[21] Note that these other techniques also typically rely upon one or more endpoint measurements, and so they face similar though sometimes less demanding luminosity hurdles. For instance, [33–35] assumed an integrated luminosity of $300\,\mathrm{fb}^{-1}$, as in the present work, in their extraction of sparticle masses at the mSUGRA [36, 37] SPS1a benchmark point [38, 39] via events with the decay chain $\tilde{q} \to \widetilde{\chi}_2^0 q \to \tilde{\ell}\ell q \to \widetilde{\chi}_2^0 \ell\ell q$ (the same chain is employed in [4, 30, 40]). A wedgebox study of the SPS1a benchmark point shows that only a simple box (with some halo events) is produced (for $300\,\mathrm{fb}^{-1}$). The wedgebox plot technique is designed to cope with points in the parameter space where more complex mixtures of decay chains occur (a possibility also touched upon in [40] – see Sect. 5.2 therein). One should always bear in mind that at the LHC one does not have the ability to scan upwards in the interaction energy to sequentially cross the various thresholds in a MSSM sparticle mass spectrum. Note also that the EW sparticle mass results at a given point in the parameter space from other invariant mass studies may well be reinforced by a contemporary wedgebox plot (constructed from either cascade neutralino pair production events as studied in [1] and/or EW production events as presented here). In addition, if m_A is sufficiently large ($m_A \gg 200\,\mathrm{GeV}$) and $\tan\beta$ intermediate ($5 \lesssim \tan\beta \lesssim 20$), corresponding to the so-called decoupling region [41, 42], then the only known potential signatures for H^0 and A^0 are via their decays into neutralino pairs [2, 3].

There are techniques that do not rely (at least not exclusively) upon endpoint measurements [43–46]. Such alternatives must make unsubstantiated assumptions about what processes and decay chains actually contribute to an observed collection of signature events. For instance, [43, 46] assume that all four-lepton signature events are from $\widetilde{\chi}_2^0\widetilde{\chi}_2^0$ production. Even then substantial amounts of integrated luminosity are required. For instance, [46] assumes $90\,\mathrm{fb}^{-1}$ at their main test point and $300\,\mathrm{fb}^{-1}$ at the SPS1a point. The popular SPS1a point is also examined in [43], again assuming $300\,\mathrm{fb}^{-1}$. The simple box topology observed at SPS1a using the wedgebox technique provides support for the assumptions made in [43, 46] *at this point in the parameter space*. Thus the development of the wedgebox plot pattern can confirm or refute assumptions required by these other techniques. Further, the wedgebox pattern may be employed to select out a subset of events that are more likely to have all come from a specific production process and decay chain to which the ideas of these alternative techniques may then be applied. For instance, selecting only events in the legs of the outer-most wedge seen on a wedgebox plot will yield a purer collection of events than selecting events from the inner-most box (which is bounded by the $\widetilde{\chi}_2^0$–$\widetilde{\chi}_1^0$ endlines but is in fact also perhaps populated by events from $\widetilde{\chi}_3^0$ and $\widetilde{\chi}_4^0$ decays).

Furthermore, commensurate with being able to compartmentalize the two-dimensional space of a wedgebox plot into a collection of simple geometrical shapes is the ability to examine the population densities in each element – for instance how many events would populate one leg of a wedge as compared to a box on the same wedgebox plot? Herein lies a true advantage of the wedgebox plot over the one-dimensional projection. Theoretically, the distribution of the population of events within a given element is expected to be fairly simple, as noted in the introduction, at least before the implementation of cuts. Thus the expected number of events in the corner box of a wedge versus the number in the legs is reasonably easy to estimate. This specifically allows us to tell whether Higgs boson $H/A \to \widetilde{\chi}_2^0\widetilde{\chi}_2^0$ production is present on top of a direct $\widetilde{\chi}_2^0\widetilde{\chi}_3^0$ channel-dominated wedge by virtue of the overpopulated corner box. Note that this information is much harder to extract from a one-dimensional projection: while the varying contributions of different production processes are reasonably clear and readily interpretable from the one-point-per pair-production-event plots in Fig. 6, this information is much harder to extract from the complex shapes of their one-dimensional projections in Fig. 9.

In other analyses examining signals for the heavier MSSM Higgs bosons (e.g., [2, 3, 22]), one typically selects a point in the MSSM IP space *and then* computes the signal rate from the Higgs boson(s) and the background rates from other MSSM processes.[22] Then if a large enough excess from the Higgs boson 'signal' is seen over the MSSM (+SM) 'background' a discovery or detection of the Higgs boson can be projected *at this point in the MSSM IP space*. But this raises the question: could the excess events attributed to the Higgs bosons at one point in the MSSM IP space be concealed in a larger SUSY background rate at another point in the MSSM IP space? This question is

[20] There is a third possibility: when one of the $\widetilde{\chi}_i^0$ decays via an on-mass-shell Z^0, the dilepton invariant mass will reconstruct to M_Z, which may be less insightful and harder to deal with due to SM backgrounds. However, it is quite rare to find a place in the viable and phenomenologically-interesting portion of the MSSM IP space where all the $\widetilde{\chi}_i^0$ decay via an on-mass-shell Z^0.

[21] Note that results presented in [4] assume integrated luminosities ranging from $10\,\mathrm{fb}^{-1}$ to $300\,\mathrm{fb}^{-1}$.

[22] Naturally SM backgrounds must also be considered, but these do not vary with the MSSM IPs.

virtually never addressed, since in these studies it would be much too computationally impractical to find the background rates at an infinite number of points spanning the whole of MSSM IP space.

Contrast this with what may be inferred from Fig. 5. As noted before, varying other MSSM IPs (in particular m_A and $\tan\beta$) whose values are constant in Fig. 5 generally does not change the major features of the plot – though the size of the islands wherein enough events are obtained may change and, on the upper island,[23] double-wedge wedgebox plots may shift into single-wedge wedgebox plots (or vice versa). This steadiness of the features in Fig. 5 allow several fairly robust conclusions to be drawn, within the context of the MSSM.

- Any box-containing wedgebox plot (including patterns with an outer box envelope, patterns with a wedge protruding from a box (as in Fig. 6a), and patterns where a box is inferred through the overpopulation of the corner of a wedge) indicates that either nature sits on the lower island in the lower corner of the (μ, M_2) plane, or events from H^0 and A^0 decays are present and substantial. The key here is the establishment that substantial direct neutralino pair production can only occur for $\widetilde{\chi}_2^0\widetilde{\chi}_3^0$ production, which yields a wedge, not a box. This also assumes cascade processes from gluino and/or squark decays yield no or very few events after cuts. This is accomplished (as checked explicitly) herein via a simple jet cut.
- The severity of the halo events, which stem from chargino and slepton production processes (especially '$3+1$' events), around the wedge and box geometries expected in the wedgebox theoretical framework indicates how near nature lies to one of the axes. High levels of such contamination are found near the axes, for low μ and/or M_2 values, while, conversely, very 'clean' wedge-like plots indicate moderate values of μ, M_2 (~ 200 GeV) and direct channel $\widetilde{\chi}_2^0\widetilde{\chi}_3^0$ domination (perhaps accompanied by contributions from H^0 and A^0 production).
- With rare exceptions, a double-wedge wedgebox plot unambiguously identifies three kinematical endpoints $M_{i1}(\ell^+\ell^-)$ $(i = 2, 3, 4)$ of neutralinos decaying through off-shell sleptons or Z^{0*}.

Ideally, one would like to make even stronger statements along the lines that if one sees a certain wedgebox pattern, this unambiguously means that one is seeing evidence for the heavier MSSM Higgs bosons, regardless of the specific point in the MSSM IP space nature has chosen. While the present analysis does not quite reach this goal, it is reasonable to expect that more detailed criteria can lead to definite conclusions concerning such issues. Nonetheless, the conclusions that may be drawn from the gross properties of wedgebox plots as herein presented are most encouraging. With the choices of where nature might lie in the MSSM IP space narrowed down by such an analysis, the full weight of more intricate probing of the data (via neural network studies and their kin [23, 24] for instance) can optimize the amount of information extractable at the LHC.

Another handle that may aid in determining if heavy MSSM Higgs bosons are generating some of the $e^+e^-\mu^+\mu^- + \not{E}$ events is the invariant mass of all four leptons combined. This is expected to be bounded above by $m_{H,A} - 2m_{\widetilde{\chi}_1^0}$ [25, 26]. However, the four-lepton (one-dimensional) invariant mass distribution will not have the abrupt turn off expected for the dilepton invariant masses plotted in the wedgebox plot [25, 26]. Studies suggest that the backgrounds and the low number of Higgs boson-generated events near the endpoint are likely to obscure detection of the endpoint. However, the shape of a histogram plotting the four-lepton invariant mass distribution may be markedly affected by having a significant fraction of the events coming from Higgs boson decays. Drawing conclusions from the distribution shape also encounters problems though, since the shape of the MSSM background (as well as that of the Higgs boson signal) varies across the MSSM IP space, again leading to the unattractive methodology of first picking a point in the parameter space and then determining if the signal + background distribution differs significantly from the background-alone distribution for this particular choice of MSSM IPs. Conclusions drawn from the wedgebox plot may help to alleviate some of this uncertainty, enabling the four-lepton invariant mass distribution to be more successfully employed.

5 Conclusions

The wedgebox technique may be used to effectively and elegantly categorize any positive outcome of an LHC search for the $e^+e^-\mu^+\mu^- + \not{E}$ signature expected from MSSM neutralino pair production. A search of the entire available MSSM IP space reveals that a sufficient number of events to make a viable wedgebox plot (somewhat arbitrarily set as being > 100) is obtained only on two 'islands' in the (μ, M_2) plane (as shown in Fig. 3). This assumes slepton masses are relatively low with $m_{\tilde{\ell}_{\rm L}} \simeq m_{\tilde{\ell}_{\rm R}}$ – if this equality is altered, then the strengthening (weakening) of sneutrino spoiler modes tends to make the islands shrink (expand) for $m_{\tilde{\ell}_{\rm L}} < m_{\tilde{\ell}_{\rm R}}$ $(m_{\tilde{\ell}_{\rm L}} > m_{\tilde{\ell}_{\rm R}})$.

Much of the lower island is already excluded by negative search results at LEP. Signature events on the small as-of-yet unexcluded portion of this island result from a mix of different production processes including a large, even dominant, component from processes involving charginos. Not unexpectedly, a number of wedgebox plot patterns result, with one pattern shifting into another fairly rapidly as the exact location in the MSSM IP space shifts. A weakness of the wedgebox plot technique is that it does not fully include charginos into its theoretical framework (at least not thus far). Nevertheless, if a wedgebox plot with a complicated structure is observed, then this points toward nature resting on this small portion of this

[23] The lower island is a domain of rapidly varying (as one moves around the IP space) wedgebox patterns which tend to be fairly complicated. This complexity serves to pinpoint the location in the parameter space as being on this lower island.

lower island. Such an observation would no doubt motivate more detailed examinations to pry more information from the rich though complicated characteristics of this already tightly-constrained region in the MSSM IP space.

The last statement is possible because of the simple character of the larger upper island: here the wedgebox pattern is remarkably constant, consisting either of a single or double wedge. This is mostly due to the fact that the only neutralino pair to be directly-produced at any appreciable rate is $\widetilde{\chi}_2^0\widetilde{\chi}_3^0$, and this yields a wedge pattern. Furthermore, unlike on the lower island, chargino production processes on the upper island are of a more tame variety, and mostly fortify the wedge structure (though halo events and sometimes Z-lines are added to the underlying wedgebox structure one hopes to categorize), while slepton backgrounds are negligible. The clarity of the double-wedge pattern on the upper island depends on whether Higgs-mediated neutralino pair production yields a sufficient number of $\widetilde{\chi}_2^0\widetilde{\chi}_4^0$ events for detection of the kinematical edge resulting from $\widetilde{\chi}_4^0 \to \widetilde{\chi}_1^0\ell^+\ell^-$ decays. Therefore if the MSSM IPs are tuned to give a very clear double-wedge pattern (i.e., at the level of Fig. 6b or better), or a wedge-protruding-from a box pattern, then one can directly read off the kinematic edges $M_{i1}(\ell^+\ell^-)$ $(i = 2, 3, 4)$ that strongly constrain the neutralino and slepton spectra and the corresponding MSSM IPs.

Another fairly sweeping general result emerges from studying the variation of the wedgebox plot patterns across the MSSM IP space: the presence of a box in a wedgebox plot, where hadronically noisy events from gluino and squark cascade decays have been removed (as shown herein), signals either chargino production or heavy Higgs boson-mediated neutralino pair production, where the former only generates suitably-resolved boxes in the quite restricted region of the MSSM IP space around $\mu, M_2 \lesssim 200\,\text{GeV}$ (i.e., the lower island). Here boxes include box-like outer envelopes to the wedgebox pattern, boxes with wedges protruding from them, and boxes identified via overpopulated lower-left corners of wedges. Compare this result to analyses that attempt to prove the presence of heavy Higgs bosons by looking for excesses in the number of expected background events from SM *and other MSSM processes* on the basis of point-by-point studies in the MSSM IP space. What, other than further typically unspecified analyses, is to say that the excess attributed to Higgs bosons at one point studied in the IP space could not be due to larger background MSSM process rates at some other unstudied point in the IP space?

Note that the above conclusions rest upon the ability to distinguish correlations between $M(e^+e^-)$ and $M(\mu^+\mu^-)$ in the wedgebox technique,[24] this being manifestly impossible in the more traditional one-dimensional invariant mass histograms like those shown in Fig. 9. Other advantages of this technique include (1) there is a one-to-one correspondence between a four-lepton event and a point on the plot, (2) asymmetries between slepton generations can be observed, and (3) better resolution of kinematic edges is possible by way of cutting out maverick and Z-line events which protrude from the dominant wedgebox shape.

This study is distinguished from most if not all of the works cited in Sect. 4 by endeavoring to encompass the overall MSSM IP space rather than just examine a single point or a few points (no attempt was made in any of the other studies cited to examine changes across any significant portion of the available parameter space). To do so though, one has had to sacrifice utilizing finely-tuned and optimized cuts and the specification of results to high precision. Thus, fully reconstructing the mass spectrum (or a portion thereof) with the associated uncertainties from the information provided by the wedgebox plot is beyond the scope of the present work. Instead, the present study seeks to map out where in the parameter space the wedgebox technique can yield salient numerical mass spectral information and the basic extent and limitations of said information. Certainly, over a large segment of the MSSM IP space the $e^+e^-\mu^+\mu^- + \not{E}$ signal rate is too low to construct a wedgebox plot.[25] Further, even if sufficient events to construct a viable wedgebox plot are found, there is no guarantee that the presence or absence of events from H^0, A^0 decays will be clearly ascertained or that the information-rich double-wedge wedgebox pattern will be produced. It is nonetheless clear that the wedgebox technique is an improvement over previous more limited analyses. It is perhaps also useful to bear in mind that nature is able to select one and only one point in the MSSM IP space, quite possibly in disregard to the 'naturalness' of large areas in this space of similar phenomenology.

Inherent in the emphasis on surveying the MSSM IP space is the ability to compare different subspaces of this parameter space. This has lead to the identification of the upper and lower islands discussed herein. Likewise, the input parameters can be repackaged to represent various schemes for SUSY-breaking within the MSSM (such as the aforementioned mSUGRA [36, 37] or GMSB [47, 48], AMSB [49–51], MIRAGE [52, 53], etc.). Wedgebox plot topologies within these different scenarios can be compared to see if the range of possible patterns overlap or not [54]. It can also be applied to the NMSSM [55–57] or USSM [58], which add a fifth neutralino. Finally, it should be emphasized that the wedgebox technique can also be employed with non-SUSY models in which pair-produced heavy exotic particles, X_iX_j, decay to dilepton pairs $X_i \to \ell^-\ell^+$. Most interesting results are obtained when there is more than one X_i so that multiple possibilities for X_iX_j – that may all be produced at varying rates in the same LHC run – exist [1]. Examples of models that may merit study include little Higgs models with T-parity [59–61] and models with extra-dimensions and a 'KK'-parity [62] or a Z_3-parity [63].

[24] It also appears possible [15] to use $e^+e^-e^+e^-$ and $\mu^+\mu^-\mu^+\mu^-$ events and use relatively simple criteria to correctly (a high percentage of the time) pair up the leptons. This will approximately double the event rates.

[25] This null result region may be reduced somewhat by considering other SM fermion–antifermion pairs in the final state, such as four same-flavor leptons as in Footnote 24 or a $b\bar{b}$ pair as in Footnote 4.

Acknowledgements. We wish to thank Ran Lu for valuable discussions and programming assistence. The authors also wish to thank Ms. S. Bauer and her coworkers at EPJC for their efforts in typesetting our paper.

This work was supported by the National Science Foundation of China (NSFC) under Grant No. 10435040 to MB.

References

1. M. Bisset, N. Kersting, J. Li, F. Moortgat, S. Moretti, Q.L. Xie, Eur. Phys. J. C **45**, 477 (2005)
2. M. Bisset, N. Kersting, J. Li, F. Moortgat, S. Moretti, hep-ph/0709.1029
3. M. Bisset, N. Kersting, J. Li, hep-ph/0709.1031
4. H. Bachacou, I. Hinchliffe, F.E. Paige, Phys. Rev. D **62**, 015 009 (2000)
5. M. Bisset, P. Roy, S. Raychaudhuri, hep-ph/9602430
6. H. Baer, X. Tata, Phys. Rev. D **47**, 2739 (1993)
7. E. Richter-Wąs, D. Froidevaux, J. Söderqvist, ATLAS Internal Note PHYS-No-108 (1997)
8. F. Gianotti, ATLAS Internal Note PHYS-No-110 (1997)
9. G. Polesello, L. Poggioli, E. Richter-Wąs, J. Söderqvist, ATLAS Internal Note PHYS-No-111 (1997)
10. J.M. Butterworth, J. Ellis, A.K. Raklev, JHEP **0705**, 033 (2007)
11. H. Baer, F.E. Paige, S.D. Protopopescu, X. Tata, hep-ph/0001086
12. H. Baer, F.E. Paige, S.D. Protopopescu, X. Tata, hep-ph/0312045
13. W.-M. Yao et al., J. Phys. G **33**, 1 (2006) [Review of Particle Physics, p. 1127]
14. H.E. Haber, G.L. Kane, Phys. Rep. **117**, 75 (1985)
15. G. Bian, M. Bisset, N. Kersting, work in progress
16. G. Corcella et al., JHEP **0101**, 010 (2001) [hep-ph/0210213]
17. S. Moretti, K. Odagiri, P. Richardson, M.H. Seymour, B.R. Webber, JHEP **0204**, 028 (2002)
18. CTEQ Collaboration, J. Pumplin et al., JHEP **0207**, 012 (2002)
19. CTEQ Collaboration, J. Pumplin et al., JHEP **0310**, 046 (2003)
20. http://www-thphys.physics.ox.ac.uk/users/PeterRichardson/HERWIG/isawig.html
21. A. Djouadi, J. Kalinowski, M. Spira, Comput. Phys. Commun. **108**, 56 (1998)
22. M. Bisset, F. Moortgat, S. Moretti, Eur. Phys. J. C **30**, 419 (2003)
23. B.P. Roe et al., Nucl. Instrum. Methods A **543**, 577 (2005)
24. H.J. Yang, B.P. Roe, J. Zhu, Nucl. Instrum. Methods A **555**, 370 (2005)
25. H. Baer, M. Bisset, D. Dicus, C. Kao, X. Tata, Phys. Rev. D **47**, 1062 (1993)
26. H. Baer, M. Bisset, C. Kao, X. Tata, Phys. Rev. D **50**, 316 (1994)
27. I. Hinchliffe, F.E. Paige, M.D. Shapiro, J. Söderqvist, W. Yao, Phys. Rev. D **55**, 5520 (1997)
28. ATLAS Detector and Physics Performance Technical Design Report 2, Chapt. 20, CERN-LHCC-99-015, ATLAS-TDR-15, http://atlas.web.cern.ch/Atlas/GROUPS/PHYSICS/TDR/access.html (May, 1999)
29. I. Hinchliffe et al., ATLAS-NOTE-Phys-109 (1997)
30. B.C. Allenbach, C.G. Lester, M.A. Parker, B.R. Webber, JHEP **0009**, 004 (2000)
31. J. Hisano, K. Kawagoe, M.M. Nojiri, Phys. Rev. D **68**, 035 007 (2003)
32. G. Weiglein et al., Phys. Rep. **426**, 47 (2006)
33. B.K. Gjelsten, D.J. Miller, P. Osland, JHEP **0412**, 003 (2004)
34. B.K. Gjelsten, D.J. Miller, P. Osland, JHEP **0506**, 015 (2005)
35. B.K. Gjelsten, D.J. Miller, P. Osland, hep-ph/0511008
36. H.P. Nilles, Phys. Rep. **110**, 1 (1984) and references therein
37. M. Drees, S.P. Martin, hep-ph/9504324
38. B.C. Allenbach et al., in: Snowmass 2001: Proc. of APS/DPF/DPB Summer Study on the Future of Particle Physics, Snowmass, Colorado, ed. by N. Graf, July, 2001, p. 125, hep-ph/0202233
39. B.C. Allenbach et al., Eur. Phys. J. C **25**, 113 (2002)
40. C.G. Lester, M.A. Parker, M.J. White, JHEP **0601**, 080 (2006)
41. S. Moretti, Pramana **60**, 369 (2003)
42. A. Djouadi, hep-ph/0503173
43. M.M. Nojiri, G. Polesello, D.R. Tovey, hep-ph/0312317
44. K. Kawagoe, M.M. Nojiri, G. Polesello, Phys. Rev. D **71**, 035 008 (2005)
45. M.M. Nojiri, hep-ph/0411127
46. H.-C. Cheng et al., 0707.0030 [hep-ph]
47. M. Dine, A.E. Nelson, Phys. Rev. D **48**, 1227 (1993)
48. C.F. Kolda, Nucl. Phys. Proc. Suppl. **62**, 266 (1998)
49. G.F. Giudice, M.A. Luty, H. Murayama, R. Rattazzi, JHEP **9812**, 027 (1998)
50. L. Randall, R. Sundrum, Nucl. Phys. B **557**, 79 (1999)
51. T. Gherghetta, G.F. Giudice, J.D. Wells, Nucl. Phys. B **559**, 27 (1999)
52. K. Choi, K.S. Jeong, K.-I. Okumura, JHEP **0509**, 039 (2005)
53. A. Falkowski, O. Lebedev, Y. Mambrini, JHEP **0511**, 034 (2005)
54. M. Bisset, N. Kersting, N. Liu, R. Lu, work in progress
55. P. Fayet, Nucl. Phys. B **90**, 104 (1975)
56. S.F. King, P.L. White, Phys. Rev. D **52**, 4183 (1995)
57. T. Elliott, S.F. King, P.L. White, Phys. Lett. B **351**, 213 (1995)
58. S.Y. Choi, H.E. Haber, J. Kalinowski, P.M. Zerwas, Nucl. Phys. B **778**, 85 (2007)
59. H.-C. Cheng, I. Low, JHEP **0309**, 051 (2003)
60. H.-C. Cheng, I. Low, JHEP **0408**, 061 (2004)
61. J. Hubisz, P. Meade, Phys. Rev. D **71**, 035 016 (2005)
62. H.-C. Cheng, K.T. Matchev, M. Schmaltz, Phys. Rev. D **66**, 056 006 (2002)
63. K. Agashe, G. Servant, Phys. Rev. Lett. **93**, 231 805 (2004)